Batteries & Supercaps

Review
doi.org/10.1002/batt.202300278

Chemistry Europe
European Chemical Societies Publishing

www.batteries-supercaps.org

Redox-Active Organic Electrode Materials for Supercapacitors

Wei Ding,[a] Luyi Xiao,[a] Li-Ping Lv,*[a, b] and Yong Wang*[a, b]

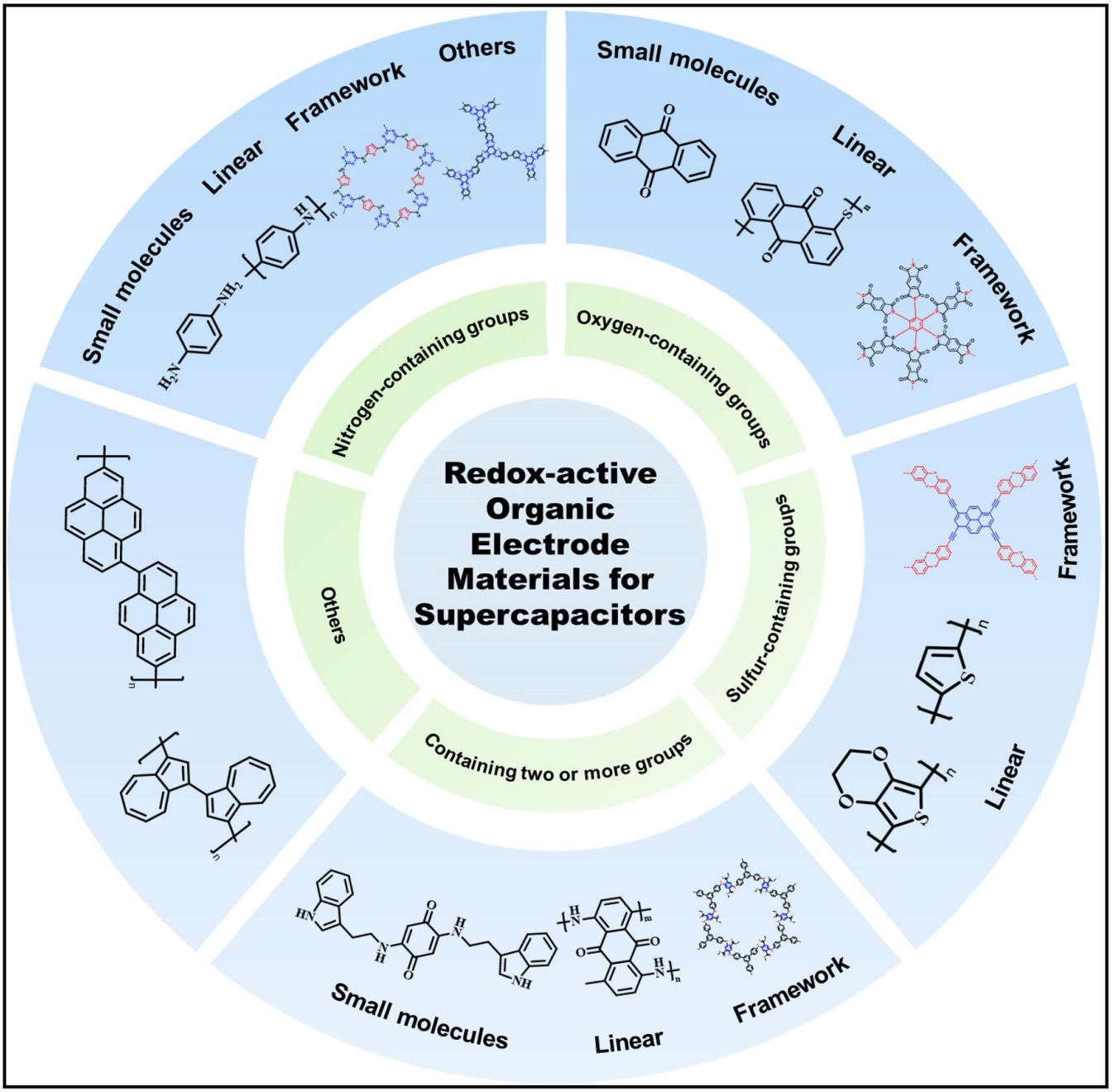

Due to their prominent power density, supercapacitors carve out a niche among all the energy storage systems. However, it is also well known that the energy density of supercapacitors takes no advantage over lithium-ion batteries, the current star energy storage device. Therefore, substantial efforts have been paid to improving the energy density of supercapacitors not at the expense of its power density. To develop electrode with high capacitance is a direct and efficient way to increase the energy storage capability of supercapacitors. Organics whose molecular structure can be diversely designed to achieve high pseudocapacitance arising from redox-active units in their backbone are good candidates as electrode materials for supercapacitors. Herein, this review summarizes recent progress of redox-active organic electrode materials for supercapacitors and their pseudocapacitive energy storge mechanisms based on different organic functional groups. From the aspects of their preparation approaches, molecular design and the resultant electrochemical performances, the focus is to probe the relationship between the energy storage mechanisms and the molecular structure of redox-active units and provide some insights for the further development of organic supercapacitor electrodes.

1. Introduction

Supercapacitors are regarded as one of energy storage systems with high application potential due to the fact that they have excellent power density relative to the current star energy storage device, lithium-ion batteries (LIBs). Nevertheless, it is also well known that the energy density of supercapacitors is relatively low (5–30 Wh kg^{-1}) which takes no advantage over LIBs (100–300 Wh kg^{-1}).[1] Therefore, substantial efforts have been paid to improving the energy density of supercapacitors without sacrifice of their power density. Among them, structural optimization of electrode materials is one of the most widely studied strategy.[2] Due to the capacitance limitation of the commercially used carbon-based electrodes which typically adopt electrical double layer-based mechanism to physically storage charges, electrode materials with the characteristics of pseudocapacitive energy storage behaviors based on surface faradaic process have attracted extensive attention.[3–5] In the case of the same working electrode material area, the pseudocapacitance can be 10–100 times higher than that of electric double layer capacitance.[6] Materials with redox-active sites such as metal oxides and conducting polymers represent two main categories of electrode materials with pseudocapacitive characteristics and have been widely investigated for supercapcacitors.[6,7] As compared to the inorganic compound-based electrode materials, redox-active organic molecules possess greater potential to be used for pseudocapacitors due to their abundant reserves, adjustable molecular structures, environmental friendliness, and the fact that they are constructed by light elements. All these merits make organic electrodes promising candidate towards supercapacitors with high energy densities.

[a] W. Ding, L. Xiao, Dr. L.-P. Lv, Prof. Dr. Y. Wang
School of Environmental and Chemical Engineering
Shanghai University
99 Shangda Road, Shanghai, 200444 (P. R. China)
E-mail: liping_lv@shu.edu.cn
yongwang@shu.edu.cn
Homepage: https://ece.shu.edu.cn/info/1144/2533.htm
[b] Dr. L.-P. Lv, Prof. Dr. Y. Wang
Key Laboratory of Organic Compound Pollution Control Engineering (MOE)
Shanghai University
99 Shangda Road, Shanghai, 200444 (P. R. China)

Among the widely studied organic electrode materials, small molecules with redox-responsive groups represent a typical category that gains detailed investigation due to their large variety and easily exposed active sites as compared to macromolecules.[8] However, they usually have fatal drawbacks of low electrical conductivity and easy dissolution in electrolytes which inevitably results in inferior energy storage efficiency and loss of the active species during long-term cycling. In contrast, organic compounds with high molecular weight, i.e., macromolecules or polymers can effectively alleviate the dissolution issue. Through introduction of pseudocapacitive groups into polymers, by polymerization of redox-active monomers or covalent bonding redox-responsive units to the as-synthesized polymer chains, the obtained polymers acquire energy storage capability and show great potential as electrode materials for supercapacitors.[2] Different from redox-active polymers that usually own low conductivity, conducting polymers such as polyaniline (PANI), polypyrrole (PPy), polythiophene (PTH) and their derivatives are also representative pseudocapacitive materials that are widely investigated as supercapacitor electrodes which has been detailed reviewed before.[9–12] Their higher conductivity as compared to most of the traditional polymers is mainly due to their conjugated structure of the backbone. Nevertheless, the conjugated chain structures conversely afford them high rigidity which is adverse for their application in electrode since the rigid polymer backbone is prone to suffering from mechanical damage upon high internal strain during charging and discharging process.

Recently, organic molecules with non-linear extended structure, for example, porous organic polymers (POPs) including covalent organic frameworks (COFs), conjugated microporous polymers (CMPs), metal organic frameworks (MOFs) etc. have attracted substantial scientific attention as electrode materials due to their structural enrichment, adjustability and porosity.[13] Similar to the linear structured polymers with redox-active units, POPs can also be well-designed to be pseudocapacitive with more exposed energy storage sites due to their high porosity and the charge transport channels in their porous structure. Nevertheless, the afore-mentioned organic electrode materials generally suffer from low electron transfer rate even for the conducting polymers or organic frameworks with conjugated structures. Therefore, most of the previously reported organic electrode with pseudocapacitive characteristics are composited with high conductive materials such as

carbon.[14] Besides, previous reports have given a broad overview of recent achievements on organic electrodes for supercapacitors. For example, Zhang et al. reviews the research progress of emerging redox polymers and conventional conducting polymers towards supercapacitor application.[15] Other recent review articles also illustrate organic electrodes for supercapacitors in detail.[2,3,16–22] However, most of these previous reviews focused on the electrochemical properties of different type of organic electrode materials or one type of organic material based on their composition mainly from the level of molecules instead of structural units that work as active sites. The classification of the energy storage mechanism arising from these active organic groups have not been described in detail.

Towards supercapacitors with high energy densities, an in-depth understanding of the pseudocapacitive features which are arising from the chemical structure of the electrode materials is necessary. Specifically, electrode materials with redox-active sites, i.e., functional units in the molecular structure that can undergo fast faradic reactions upon electrochemical charging/discharging, are highly demanding and have attracted enormous research efforts. The importance of the relationship between the energy storage mechanism and structures can be therefore reflected by the fact that different active groups in the chemical structures of the electrode materials possess distinctive reaction kinetics which involves charge transfer and ion diffusion process occur on the electrodes and decides the energy storage capacitance of the electrode. Herein in the present review, we classify the organic electrode materials based on the redox-active units in their structure. Heteroatoms such as O, N and S contain lone pair electrons and O, N and S-containing groups especially those with unsaturated bonds for example carbonyl (–C=O) and imine groups (C=N), can act as redox-active sites to store charges during the charge/discharge process through structural interconversion. Indeed, a large number of organic molecules containing such electrochemically active groups in their chemical structures have been successfully synthesized and used as pseudocapacitive electrode materials. Moreover, when these active groups are present in molecules with different characteristics including molecular weight, conjugated extent, microstructures and so on, their redox-active behaviors change which consequently affects the electrode reactions and then the electrochemical performance of the organic materials.

Herein, we summarize organic materials more comprehensively with both low molecular weights, i.e., the redox-active small molecules and high molecular weight, i.e., the redox-active polymers. The latter is further classified into linear polymers, and polymers with non-linear extended structures, including framework-structured COFs, MOFs and other POPs that are not framework-structured. When present these redox-active molecules, we classify them according to different active groups that work as energy storage units in supercapacitors and demonstrate the relationship between the redox activities of these chemical groups and their pseudocapacitive properties. Based on the previously reported works on pseudocapacitive organic electrode materials, we divide these active groups into O, N, or/and S-containing groups since each type often adopts similar energy storage mechanisms. The summary of organic electrode materials based on different active groups in the present review may provide a more explicit suggestion for the rational design of redox-active pseudocapacitive materials.

2. Pseudocapacitive Electrode Materials based on Different Active Groups

In this part, we mainly summarize different organic electrode materials owning pseudocapacitive features through redox reactions occurring in O-containing groups, N-containing groups, S-containing groups, and functional groups containing

Wei Ding received her B.Sc in 2017 majoring in Chemical Engineering and Technology from Yancheng Institute of Technology. Currently, she is pursuing her M.S. degree in the School of Environmental and Chemical Engineering at Shanghai University. Her research interests focus on organic electrode materials for supercapacitors, flexible wearable supercapacitors.

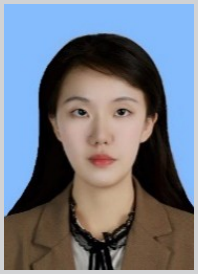

Luyi Xiao received her Bachelor's degree in Applied Chemistry from Shanghai Institute of Technology of Applied Sciences in 2018. Currently, she is pursuing her Master's degree in the School of Environmental and Chemical Engineering at Shanghai University. Her research interests focus on organic electrodes and self-healing hydrogel electrolytes for supercapacitors.

Li-Ping Lv obtained her doctor's degree at Max Planck Institute for Polymer Research in 2014. She joined School of Environmental and Chemical Engineering of Shanghai University in 2015 and was appointed as an associate Professor since 2019. Her research interests focus on the design of functional nanomaterials and their applications in energy storage and environmental protection.

Yong Wang obtained his doctor's degree in Chemical Engineering at National University of Singapore in 2004. He worked as a research fellow in Singapore - Massachusetts Institute of Technology Alliances from 2004 to 2006. He joined Shanghai University and was appointed as a professor in 2007. He is currently the executive vice dean of School of Environmental and Chemical Engineering of Shanghai University. His research interests focus on materials for energy storage and environment.

Review
doi.org/10.1002/batt.202300278
Chemistry Europe
European Chemical Societies Publishing

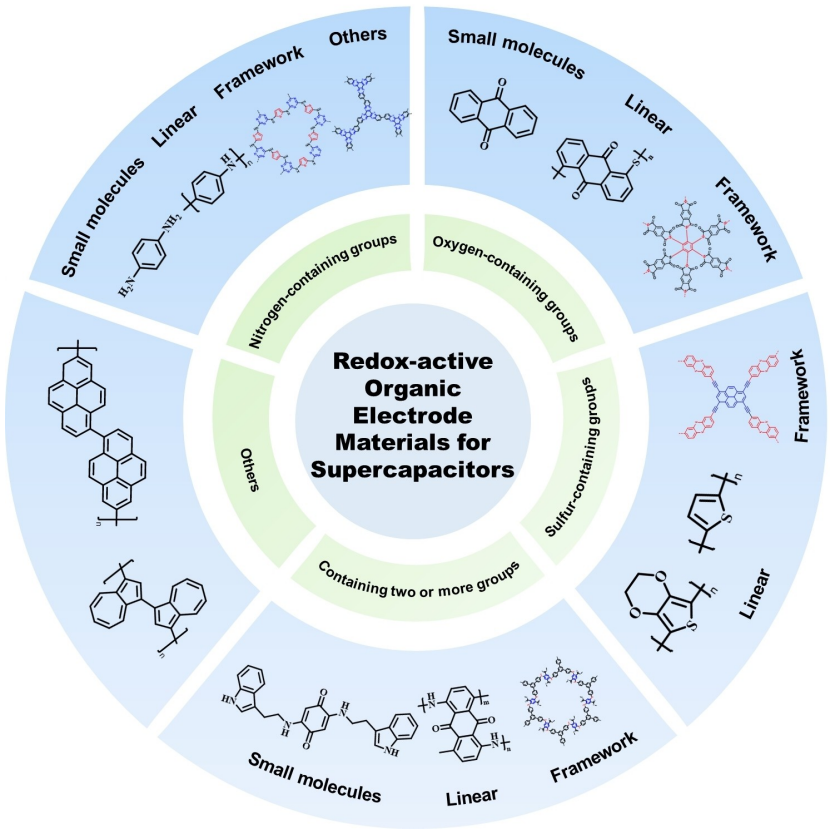

Figure 1. Redox-active organic electrode materials for supercapacitors.

two or more groups and others (Figure 1). Then in each section, we further divide them into small molecules, linear polymers, and structure-extended polymers, considering that the electrochemical behaviors of these organic molecules with different sizes vary which may reflect the following aspects: first, small molecules are susceptible and more easily dissolve in electrolytes during redox processes, leading to inferior cyclability of the electrode compared to polymer-based molecules containing same redox-active unit. Furthermore, one-dimensional linear polymers often suffer from structural collapse due to the doping/de-doping of electrolyte ions during redox processes. In comparison, polymers with extended structures may alleviate both the dissolution problem of small molecules and the issue of structural instability of linear polymers. Second, the vast majority of small molecules are insulating due to their short molecular chains therefore restricted pathways for electron transport. Whereas for the polymeric materials with elongated and extended structures, conjugated systems consisting of large π-bonds can be achieved with redox activity of the functional groups activated to donate improved pseudocapacitance.

In addition to different molecular sizes, polymers with extended structure are further classified into framework and non-framework structured ones, with the consideration that structural differences for example porosity and crystallization also affect the energy storage process of these electrode materials. The categories of framework structure COFs, MOFs and other POPs that are not framework-structured are included. Note that MOFs are not necessarily classified as organic electrode materials if different energy storage mechanisms arising from their metal centers or the organic ligands are considered. When their organic linkers work as the active units for charge storage in supercapacitors, these MOFs are regarded as organic electrode materials. Therefore, for the MOF structures, we only summarize the works with the redox processes occurring in the organic ligands, which is relatively less reported and mainly studied with nitrogen-containing functional groups.

2.1. Oxygen-containing groups

The most common and widely reported oxygen-containing group in organic materials for energy storage is carbonyl group (–C=O). For each carbonyl group, it can store an electron while inserting a cation or a proton (Figure 2). Most carbonyl-

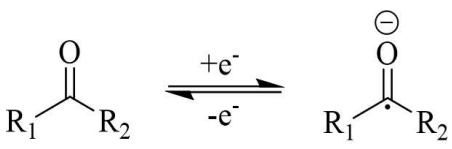

Figure 2. Mechanism of redox reaction of carbonyl groups.

containing organic compounds participate in redox processes with an even number of carbonyl groups. Take 1,4-benzoquinone (BQ) containing two carbonyl groups as an example, during reduction, one electron is injected into the BQ molecule while one carbon-oxygen π-bond breaks to produce a radical anion intermediate (also known as a semi-quinone intermediate). With the injection of the second electron, another carbon-oxygen π-bond breaks, and the newly emerged single electron can pair with the previous single electron to form a divalent ion as the final discharge product. Generally, the cation in the electrolyte will combine with the radical anion intermediate and the divalent anion product to compensate for the charge.[23]

2.1.1. Small molecules

Redox-active small organic molecules are potential electrode materials for supercapacitors due to their wide varieties, good sustainability, and high redox reversibility.[24] However, they are usually not independently used as electrode materials owing to their poor electrical conductivity and easy dissolution in electrolytes, which limits their rapid development in supercapacitors. Studies have shown that immobilizing redox-active small organic molecules on conductive carbon substrates such as graphene, carbon nanotubes, activated carbon, etc. can promote the charge transfer from electroactive molecules to current-carrying elements, improving the performance of electrochemical energy storage devices, power capability, and effectively exert their electrochemical performance.[25]

Regarding the features of electrolytes for small molecule-based electrodes, there are far more reports using acidic electrolyte other than alkaline electrolytes. Small molecules containing oxygen functional groups that work with neutral electrolytes are rarely reported in supercapacitors. The possible reason might be that the specific capacitance of the small organic molecules measured in acidic electrolytes is generally greater than that in neutral/alkaline electrolytes. Specifically, the efficiency of aqueous electrolytes depends mainly on the mobility of the ions and the size of the hydrated ions, which affect the ionic conductivity and ultimately the specific capacitance. The ionic conductivity of H_2SO_4 at 25 °C, for example, was 0.8 S cm^{-1}, which is higher than that of the alkaline electrolyte (0.6 S cm^{-1} for 6 M KOH at 25 °C) and the neutral electrolyte (e.g., 0.5 S cm^{-1} for 1 M Na_2SO_4 at 25 °C).[26,27] Moreover, the pH of the electrolytes does have some effect on the dissolution of organic materials especially small molecules. Yan et al. investigated the solubility of anthraquinone (AQ) in neutral electrolytes (1 M LiCl, NaCl, KCl, $CaCl_2$ and $BaCl_2$ of aqueous solutions) for redox processes. The AQ molecule was found to undergo a one-electron redox reaction to generate the radical anion $[AQ]^-$, and then $[AQ]^-$ interacts with metal ions to generate $[AQ–M^{n+}]^{(n-1)+}$, which is readily soluble in the electrolyte, leading to a poor redox reversibility of the electrode. However, under acidic conditions, AQ underwent two-electron redox reactions in 1 M $AlCl_3$, $MgCl_2$ and $ZnCl_2$ electrolytes. Due to the easily happened substitution reaction between anthracene hydroquinone (AQH_2) and metal ions, the reversible redox reactions at the electrode then can be fully realized.[28]

Extensive studies have shown that quinone-based small molecules can undergo reversible redox reactions and provide pseudocapacitance for supercapacitors. The following Table 1 summarizes the recently reported quinone-based small molecule as electrode materials in supercapacitors. Note that there are effects of the two or three electrode systems on the capacitance measurements. The effects can be arising from, for example, the geometry of the substrates on which the active materials are deposited, the loading mass, the type of electrolytes and so on. Moreover, the measured specific capacitance of the electrode material in the three-electrode system is approximately the same as that of the working electrode because the counter electrode is considered to be ideal, the system is infinitely electronic, and the concentration in the solution is infinitely constant. However, when pseudocapacitive materials are assembled into a two-electrode system, i.e., a supercapacitor device, power consumption will occur leading to a much lower tested specific capacitance.

Quinones are a class of organic compounds with a six-membered cyclic diketone (containing two carbonyls) structure containing two double bonds. Faraday process occurs mainly based on the redox reaction of quinone groups. Upon reduction, quinone combines two protons and two electrons in acidic electrolyte or combines two electrons and cationic substance in basic electrolyte,[29] as shown for AQ in Figure 3.

In 2004, Leitner et al. first applied quinone-modified carbon electrode into capacitors. When using 1,2-naphthahydroquinone to modify carbon material with high surface area, the redox contribution of this quinone-based organic molecule to the total stored charges was estimated to be 126 C g^{-1}. The double layer capacitance of carbon was not affected by the addition of quinone molecules and less than 20% of capacitance loss was observed after 1000 charge/discharge cycles.[30]

In addition to compound redox-active small molecules with carbons to improve their electrochemical performances, it is also important to select suitable redox-active molecules on positive and negative electrodes. To be specific, for the negative electrode, the carbon material combined with small molecules should have a voltage window as close as possible to the cathodic limit potential, and conversely, that of the positive electrode should be close to the anodic limit potential in the

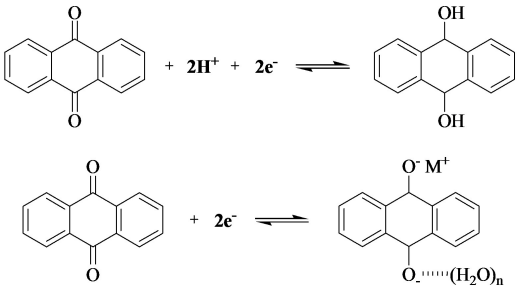

Figure 3. Redox reactions of anthraquinone in acidic (top) and alkaline (bottom) electrolytes.[29]

Table 1. Electrode materials based on small molecules containing oxygen functional groups.

Materials	Preparation	Electrolytes	Specific capacitance, current density	Capacity retention, Cycle number	Energy density [Wh kg^{-1}], power density [W kg^{-1}] (two-electrode)	Electrode system	Ref.
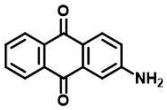 (N-RGO@AAQ)	solvothermal method	1 M H_2SO_4	532.48 C g^{-1} at 0.6 A g^{-1}	94.67% (18000, 30 mV s^{-1}) (two-electrode)	21.13, 750	three	[40]
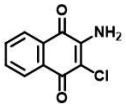 (2-NTQ-RGO)	covalent reaction	1 M H_2SO_4	453 F g^{-1} at 1 A g^{-1}	83% (8000)	16.7, 812	three	[41]
 (NQ-rGO/CF)	hydrothermal self-assembly	5 M KOH	223.8 F g^{-1} at 0.21 A g^{-1}	87% (10000)	50.7, 204	three	[42]
 (KB/DCBQ)	solvent-free method	1 M H_2SO_4	146 F cm^{-3}	10000	/	three	[43]
 (P-BQ/C)	dipping method	0.5 M H_2SO_4	350 F g^{-1} at 10 mV s^{-1}	93.5% (5000)	/	three	[44]
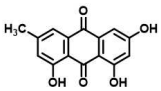 (E@GNS)	sonication	1 M H_2SO_4	338.9 F g^{-1} at 5 mV s^{-1}	80.3% (7000, 5 A g^{-1})	32.8, 800	three	[45]
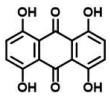 (THAQ/rGO)	one-step hydrothermal synthesis	1 M H_2SO_4	259 F g^{-1} at 1 A g^{-1}	97.9% (10000)	/	three	[46]
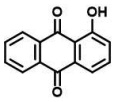 (HAQ-rDCNTs)	solution processing	1 M H_2SO_4	324 F g^{-1} at 1 A g^{-1}	/	12.3, 700	three	[47]
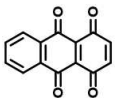 (C-AT)	dipping method	0.5 M H_2SO_4	/	90% (1000)	/	three	[48]
 (Catechol-C)	sonication	1 M H_2SO_4	250 F g^{-1} at 2 mV s^{-1}	98.5% (1000)	/	three	[36]
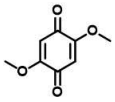 (DMQ-rGO)	one-step hydrothermal synthesis	1 M H_2SO_4	650 F g^{-1} at 5 mV s^{-1}	99% (25000)	/	three	[25]

Table 1. continued

Materials	Preparation	Electrolytes	Specific capacitance, current density	Capacity retention, Cycle number	Energy density [Wh kg^{-1}], power density [W kg^{-1}] (two-electrode)	Electrode system	Ref.
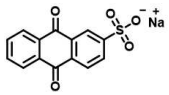 (AQS-rGO)	hydrothermal	1 M H_2SO_4	567.1 F g^{-1} at 1 A g^{-1}	10 A g^{-1}, 89.1% (10000)	29.2, 21600	three	[49]
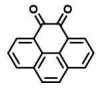 (4,5-Pyrenedione-carbon onion)	sonication	1 M H_2SO_4	264 F g^{-1} at 5 mV s^{-1}	97% (10000)	/	three	[34]
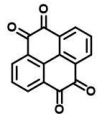 (PYT/GN)	non-covalent reaction	1 M H_2SO_4	711 F g^{-1} at 1 A g^{-1}	91.4% (5000, 3 A g^{-1}) (two-electrode)	18.4,700	three	[50]
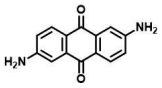 (DQ-RGO)	nucleophilic displacement reaction	1 M H_2SO_4	332 F g^{-1} at 1 A g^{-1}	81.8% (5000)	14.2, 763	three	[51]
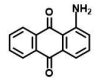 (1-AAQ-CC2)	solvothermal method	2 M KOH	328 F g^{-1} at 0.5 A g^{-1}	95% (5000)	14.8, 240	three	[52]
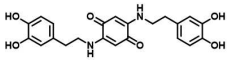 (BQ-DP-graphite sheet)	covalent reaction	1 M H_2SO_4	1180 F g^{-1} at 9.5 A g^{-1}	70.6% (5000)	/	three	[53]
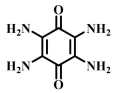 (TABQ-MWCNT)	solvothermal	1 M H_2SO_4	463 F g^{-1} at 1 A g^{-1}	76.8% (6000, 10 A g^{-1})	15.6, 700	three	[39]
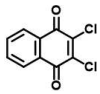 (2-DCTQ/RGO//2-DCTQ/RGO)	non-covalent reaction	1 M H_2SO_4	100 F g^{-1} at 1 A g^{-1}	65% (5000, 5 A g^{-1}) (three-electrode)	45, 0.91	two	[54]
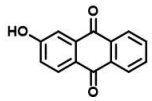 (HAQ-rGO)	solvothermal reaction	1 M H_2SO_4	64.9 F g^{-1} at 1 A g^{-1}	86% (10000, 10 A g^{-1})	17.7, 700	two	[55]
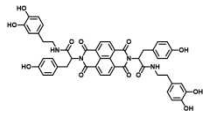 (NDI-Tyr-DP)	covalent reaction	1 M H_2SO_4	85 F g^{-1} at 0.5 A g^{-1}	77.10% (5000)	10.63, 899	two	[56]
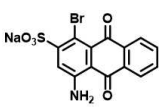 ($Ti_3C_2T_x$-ABS)	non-covalent reaction	1 M H_2SO_4	1686.72 mF cm^{-2} at 0.25 mA cm^{-2}	137% (40000)	599.72 mWh cm^{-2}, 200 mW cm^{-2}	two	[38]

Table 1. continued

Materials	Preparation	Electrolytes	Specific capacitance, current density	Capacity retention, Cycle number	Energy density [Wh kg^{-1}], power density [W kg^{-1}] (two-electrode)	Electrode system	Ref.
  (A-HC/DCAQ)(A-HC/TCBQ)	grind	0.5 M H_2SO_4	/	91.0% (1000)	19.0, 45500	two	[57]
  (AQ/NPC)(TCBQ-NQ/NPC)	sonication	1 M H_2SO_4	86 F g^{-1} at 1 A g^{-1}	75.3% (5000)	23.5, 700	two	[58]
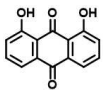 (DT-CRGNs)	one-step re-melting	1 M H_2SO_4	284.8 F g^{-1} at 1 A g^{-1}	92.4% (10000)	12.6, 700	two	[59]
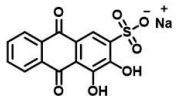 (ARS-PEDOT/CFs)	post-processing	1 mg mL^{-1} ARS	488.9 F g^{-1} at 5 mV cm^{-2}	82.21% (1000)	4.87 mWh cm^{-3}, 36 mW cm^{-3}	two	[60]
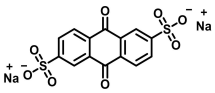 (RGO-AQDS)	hydrothermal	1 M H_2SO_4	398.5 F g^{-1} at 1 A g^{-1}	82% (10000)	52.24, 1000	two	[61]
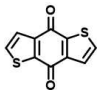 (BDTD-rGO)	one-step solvothermal method	1 M H_2SO_4	54 F g^{-1} at 1 A g^{-1}	81.3% (8000)	9.52, 450	two	[33]
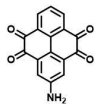 (PYT-NH_2/rGO)	solvothermal method	1 M H_2SO_4	77.2 F g^{-1} at 0.5 A g^{-1}	100% (25000)	15.4, 182.2	two	[37]
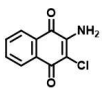 (CNQ-GNS)	a single-step reflux method	1 M H_2SO_4	53.8 ± 4 F g^{-1} at 1 A g^{-1}	100% (10000)	19.1, 800	two	[35]

electrolyte.[31] For example, Guo et al. prepared quinone-functionalized carbons (TCBQ–NHC and AQ–NHC) through adsorption of TCBQ or AQ molecules on the N-doped carbon via π–π stacking interaction. The TCBQ–NHC and AQ–NHC electrodes reached specific capacitances of 365 and 331 F g^{-1} at 1 A g^{-1} in the potential windows of 0–1.0 and −0.4–0.6 V and the capacitance retention retained 96% and 81% after 5000 cycles at 10 A g^{-1}, respectively. Moreover, the assembled AQ–NHC//TCBQ–NHC asymmetric supercapacitor (ASC) showed an energy density of 20.3 Wh kg^{-1} at the power density of 0.7 kW kg^{-1} and retained 98% of the capacitance after 5000 cycles.[32]

Besides, the structure, conjugation characteristics, and electronic properties are also important to improve the capacitance and cycle life of the quinone-based electrode.[33] Anjos et al. compared the energy storage performance of three

different small molecules (1,4-naphthoquinone, 9,10-phenanthrenequinone, and 4,5-pyrenedione) compounded with carbon onions. Due to their different molecular structures, the 4,5-pyrenedione having the largest binding energy to the onion-like carbon (OLC) exhibited the best electrochemical performance, i.e., a maximum capacitance of 264 $F g^{-1}$ (5 $mV s^{-1}$) and a specific capacitance retention of 97% after 10000 cycles at 1.3 $A g^{-1}$.[34] Boota et al. prepared a redox-active dry gel by modifying 2,5-dimethoxy-1,4-benzoquinone (DMQ) on reduced graphene oxide (rGO) sheets via a hydrothermal method. The composite showed a specific capacitance of 650 $F g^{-1}$ at 5 $mV s^{-1}$ in 1 M H_2SO_4 and maintained 99% of the initial value after 25000 cycles at 50 $mV s^{-1}$. DMQ can not only provide stable redox-active centers but also act as a spacer to alleviate the aggregation of rGO sheets to form a three-dimensional (3D) layered electrode.[25] Li et al. synthesized three-dimensionally interconnected benzo 1,2-b:4,5-b-dithiophene-4,8-dione (BDTD)-functionalized dry gels (BDTD-rGO) via a one-step solvothermal method. BDTD is a planar molecule with a fused heterocyclic aromatic structure which makes it adsorbed on rGO via π–π interactions. Since the five-membered aromatic heterocycle is more electron-rich than the six-membered aromatic ring, it helps increase the electron interaction between BDTD and the conjugated graphene and reduce the solubility of the BDTD in electrolytes. The composite consequently achieved a high specific capacitance of 360 $F g^{-1}$ and an enhanced cycle stability with 96.4% of capacitance retention after 10000 cycles.[33]

Note that most of the reported quinone-based small molecules are compounded with carbon materials through non-covalent interactions (π–π interactions, hydrogen bonding, etc.). These weak non-covalent interactions cannot effectively avoid the dissolution of the organic molecules on electrodes into the electrolyte, eventually leading to poor cycle life.[14] Moreover, the volume change during the charge/discharge cycle also leads to the rapid degradation of the electrode performance. Therefore, the covalent functionalization strategy is expected to be an efficient way to solve these problems. Organic small molecules are bonded to carbon materials through covalent bonds. The strong covalent force can then prevent the dissolution of small molecules, thus improving the cyclic stability of the composites while maintaining high capacitance.[35] Pognon et al. covalently functionalized activated carbon with catechol diazonium ions (Figure 4a). The composite electrode well combines the Faraday capacitance arising from the surface-immobilized catechol moiety and the electrochemical double-layer capacitance from black pearl carbon with high surface area. The catechol-modified electrode obtained a higher specific capacitance (250 $F g^{-1}$) than that of the pristine carbon (150 $F g^{-1}$) with a voltage window of −0.4 to 0.75 V in 1 M H_2SO_4. Furthermore, the covalently cross-linked catechol-modified carbon showed a small decrease in capacitance compared to the non-covalently cross-linked one after 10000 constant current charge/discharge cycles.[36] Shi et al. designed an organic small molecule 2-aminepyrene-3,4,9,10-tetrone (PYT–NH_2) (Figure 4b), which was anchored to GO by covalent bonding and then further reduced to PYT–NH_2/rGO. The composite PYT–NH_2/rGO achieved a specific capacitance of 326 $F g^{-1}$ at 0.5 $A g^{-1}$ and the capacitance retention of the assembled asymmetric supercapacitor AC//PYT–NH_2/rGO is close to 100% at 5 $A g^{-1}$ after 25000 cycles.[37] Zhang et al. cross-linked MXene with 1-hydroxyanthraquinone (HA) and 1-amino-4-bromoanthraquinone-2-sodium sulfonate (ABS) through covalent bonding (Figure 4c). The formed amino ester can form a p-π conjugated structure with the electron cloud on the benzene ring to improve the electrode electrical conductivity. Further-

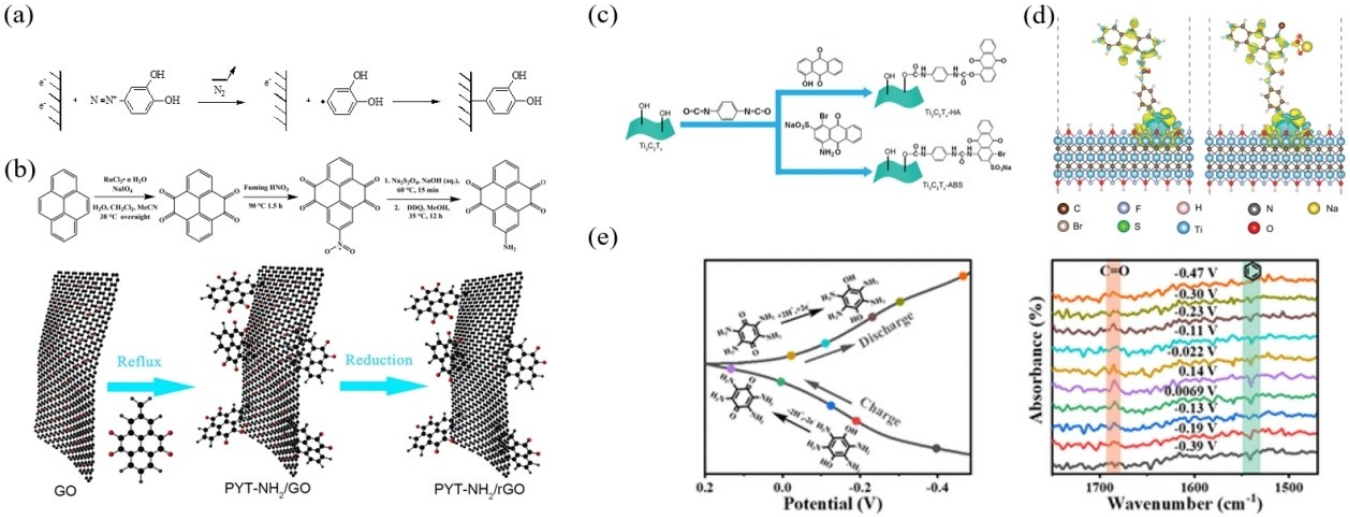

Figure 4. a) Synthesis routes of Catechol-C composite. Adapted from Ref. [36] Copyright (2012) American Chemical Society. b) Synthesis routes of PYT–NH_2 and PYT–NH_2/rGO composite. Adapted from Ref. [37] Copyright (2018) American Chemical Society. c) Schematic diagram of titanium carbide covalently cross-linked with HA (or ABS) to prepare $Ti_3C_2T_x$–HA (or $Ti_3C_2T_x$–ABS). Adapted from Ref. [38] Copyright (2022) Wiley-VCH GmbH. d) DFT simulation of the relationship between structural and electrochemical properties of Titanium carbide- HA (left) and Titanium carbide-ABS (right). Adapted from Ref. [38] Copyright (2022) Wiley-VCH GmbH. e) In situ FTIR spectral evolutions of TABQ-MWCNTs during charging and discharging. Adapted from Ref. [39] Copyright (2022) American Chemical Society.

more, ABS introduces electron-accepting groups to regulate the redox potential of the electrode (Figure 4d). It was predicted to enhance the electronic conductivity of the covalently cross-linked structure, thus improving the multiplicative performance of the electrode. The assembled asymmetric device Titanium carbide–ABS//AC finally achieved an area specific capacity of 1686.72 mF cm^{-2} at 0.25 mA cm^{-2} with the specific capacity decreased only slightly as the current density gradual increased.[38] Our group prepared 2,3,5,6-tetraamino-p-benzoquinone-multi-walled carbon nanotube (TABQ-MWCNTs) composites by a simple hydrothermal reaction. The small molecules TABQ were anchored on the surface of MWCNTs through π–π stacking between TABQ and the large π bonds in MWCNTs, forming a stable structure. In addition, the hydrogen bonds formed between the hydroxyl groups on MWCNTs and the amino groups on TABQ further enhanced the structural stability of the TABQ-MWCNTs composites. In-situ FTIR (Figure 4e) showed an intensity increase/decrease of C=O arising from TABQ during charging/discharging process, verifying the pseudocapacitance donated by TABQ through faradic reactions. The obtained redox-active TABQ-MWCNT composites then exhibited good electrochemical properties, with a high specific capacitance of 463 F g^{-1} at 1 A g^{-1} and an initial capacitance of 76.8% obtained after 6000 cycles at 10 A g^{-1}. The assembled asymmetric supercapacitor (ASC) with TABQ-MWCNTs//activated carbon has an energy density of 15.6 Wh kg^{-1} at a power density of 700 W kg^{-1}. In addition, the initial specific capacitance of 91.5% was maintained after 10000 cycles at 5 A g^{-1}.[39]

2.1.2. Linear-structured polymers

Linear-structured polymers can be generally obtained through polymerization of small molecules which we call monomers. Due to the covalent bonding of monomer units in a linear way, the formed polymer chains are linear-structured and gain higher stability as-compared to their small molecule counterparts. Indeed, molecules with low molecular weight are easier to dissolve into the electrolyte compared to macromolecules due to the strong interaction between their short chains with the electrolyte compared to polymers with long entangled chains. Besides, in contrast to small molecules which are usually electronic insulating due to the limited transportation for the electrons in the molecular structure, linear-structured polymers can be designed to be conducting through their extended conjugated chains. Examples include the traditional conducting polymers like polyaniline, polypyrrole, polythiophene and so on. Moreover, these conducting polymers can be further doped to enhance their electrical conductivity and accelerate electron transport which facilitate the charging and discharging process when used as electrode materials. The charge storage mechanism of these linear polymers can be mainly classified into p-type (p-doping) and n-type (n-doping) (Figure 5), where p-doping implies that the polymer undergoes an oxidation reaction by extracting electrons from its original neutral state to produce a positively charged state, followed by a reversible reduction reaction. Conversely, n-doping indicates that the polymer is subjected to reduction by accepting electrons, resulting in a negatively charged state, which is then oxidized back to its initial state.[62] Note that there is also a case where

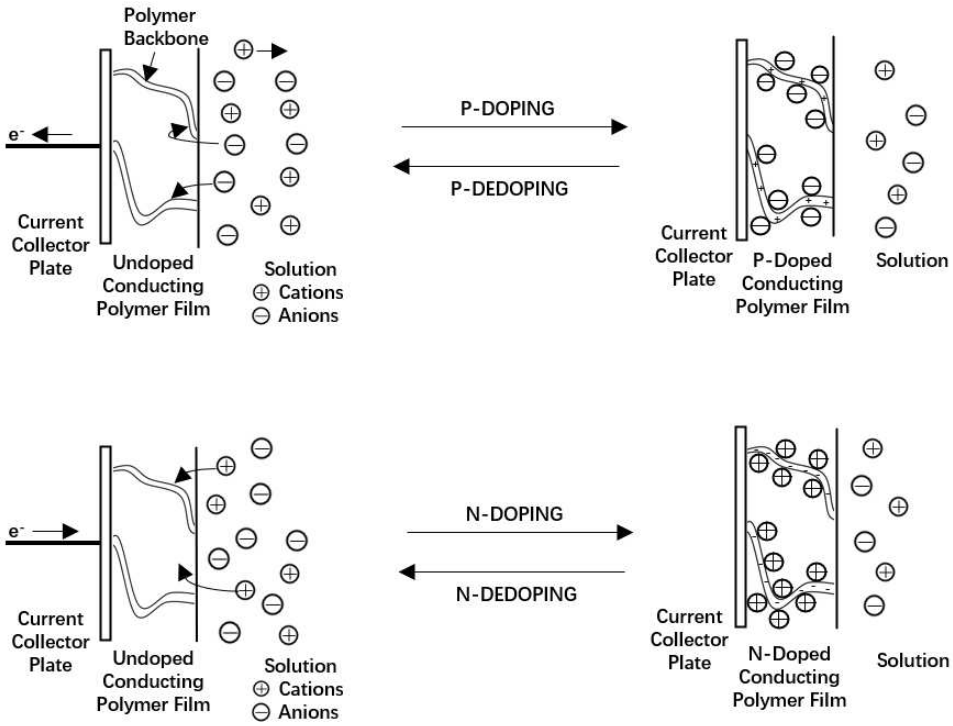

Figure 5. A schematic representation of the charging and discharging processes at conducting polymer electrodes associated with p-doping and n-doping. Reproduced with permission from Ref. [62] Copyright (1994) Elsevier B.V.

the polymer is able to carry positive and negative charges from its natural state through oxidation and reduction processes, respectively, which is called bipolar doping.[15] It means that both n-doping and p-doping can occur in the bipolar doping polymers, but not simultaneously. In another word, the electrode with bipolar doping properties can undergo both n-doping to act as a negative electrode and p-doping to act as a positive electrode.

Previous research has shown that linear polymers containing oxygen-functional groups can work as redox-active centers for energy storage. For example, in 2014, Lee et al. synthesized poly(anthraquinonyl sulfide) (PAQS)/graphene sheet (GSs) composites by in situ polymerization. The PARQ electrode obtained a specific capacitance of 349 $F g^{-1}$ (86 $mAh g^{-1}$) at a current density of 0.5 $A g^{-1}$.[63] This high energy storage capability is also mainly attributed to the redox reaction of carbonyl groups (Figure 6), Two carbonyl groups act as electron acceptor and transform to hydroxyl groups in the presence of protons.

2.1.3. Porous organic polymers (POPs)

2.1.3.1. Framework structured POPs-COFs

COFs are a new type of POPs with a molecularly ordered structure formed by covalently linked organic structural units.[64] Basically, the structure of a COF consists of linkers (building blocks) and links (bonds between building blocks). Owing to the wide variety of reaction types and high availability of building blocks, COF materials with a wide range of structures and properties can be prepared through varying the reaction types (mainly including coupling reactions and oxidative polymerization synthesis[65]) and changing different building blocks.[1] To design COFs-based pseudocapacitive electrode materials in supercapacitors, the utilization of redox-active linkers as building blocks is regarded as a common approach.

In 2013, the group of Dichtel reported the first use of COF in supercapacitors. The COF was synthesized by the redox-active monomer 2,6-diamineanthraquinone and 1,3,5-tricarbonylresorcinol. The presence of quinone redox-active units endows the electrode material with electrochemical properties, the initial capacitance of the DAAQ-TFP COF-modified electrode was 48 ± 10 $F g^{-1}$ and was maintained at 40 ± 9 $F g^{-1}$ after 5000 charge/discharge cycles.[66] Among COFs used in supercapacitors with redox properties, the ones with O-containing groups especially carbonyl structure are representative. Table 2 summarizes the COF materials containing oxygen functional groups used in supercapacitors.[67–71] Li et al. designed four COF materials via Schiff base condensation reactions using 2,4,6-tricarbonylresorcinol (Tp) as the node and a series of biphasic diamines as the reaction monomer (each joint unit of the series of biphasic diamines contains no, one, two, and four KT parts, respectively), as is shown in Figure 7. The energy storage mechanism corresponds to the redox reactions of the quinone groups in the joint units. The obtained 4KT–Tp COF electrodes exhibited a high capacitance of 583 $F g^{-1}$ at 0.2 $A g^{-1}$ and achieved above 92% of capacitance retention even after 20000 cycles at 5 $A g^{-1}$.[70] Halder et al. prepared flexible self-supporting TPOMe-DAQ by simple grinding method. The TPOMe-DAQ exhibited an excellent area capacitance of 1600 $mF cm^{-2}$ (169 $F g^{-1}$) and cycling stability ($>$100000 cycles). The assembled symmetric solid-state supercapacitor device can

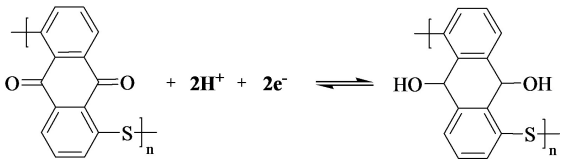

Figure 6. Mechanism of redox reaction of PAQS.

Table 2. Electrode materials based on framework-structured polymers containing oxygen-functional groups.

Materials	Preparation	Specific capacitance, current density	Capacity retention, Cycle number	Energy density [$Wh kg^{-1}$], power density [$W kg^{-1}$] (two-electrode)	Electrode system	Ref.
DAAQ-COFs	cationic driven electrostatic self-assembly method	390 $F g^{-1}$ at 0.5 $A g^{-1}$	88.9 (20000)	27.5, 350	three	[76]
Dq_1Da_1Tp	grind	122 $F g^{-1}$ at 1.56 $mA cm^{-2}$	90% (2500)	/	three	[68]
4KT-Tp COFs	Schiff-base polycondensation	583 $F g^{-1}$ at 0.2 $A g^{-1}$	92% (20000, 5 $A g^{-1}$)	/	three	[70]
TpOMe-DAQ	grind	1280 $mF cm^{-2}$ at 10 $mA cm^{-2}$	/	2.9 $\mu Wh cm^{-2}$, 61.8 $\mu W cm^{-2}$	three	[69]
TpPa-$(OH)_2$	Schiff-base polycondensations	416 $F g^{-1}$ at 0.5 $A g^{-1}$	66% (10000, 5 $A g^{-1}$)	/	three	[67]
PAQTA	Buchwald-Hartwig coupling	576 $F g^{-1}$ at 1 $A g^{-1}$	80% (6000, 2 $A g^{-1}$)	60, 1300	three	[77]
P1	solvothermal reaction	805 $F g^{-1}$ at 0.5 $A g^{-1}$	/	/	three	[78]
CPI@CA	support coating strategy	1600 $F g^{-1}$ at 5 $mV s^{-1}$	90% (10000, 100 $A g^{-1}$, two-electrode)	94, 1066	three	[79]
TAT-CMP-2	Schiff-base polycondensation	183 $F g^{-1}$ at 1.0 $A g^{-1}$	95% (10000, 10 $A g^{-1}$)	/	three	[77]

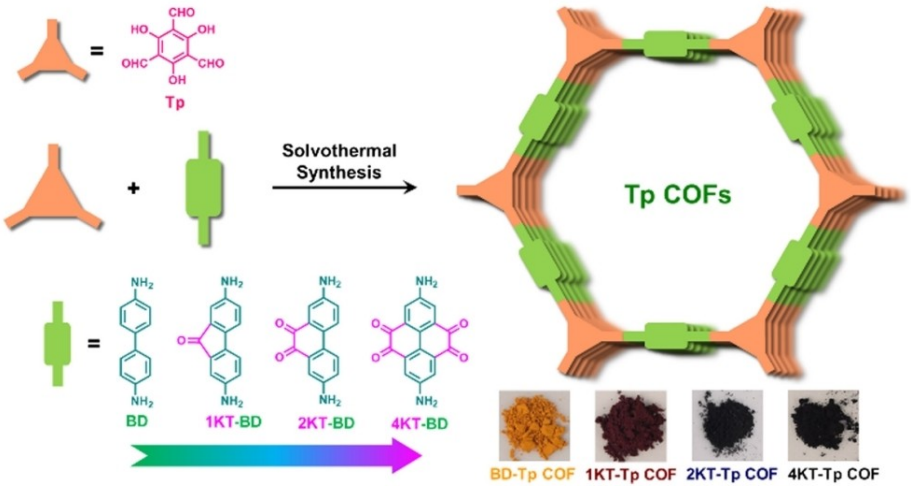

Figure 7. Schematic illustration of the design and synthesis of Tp COFs via skeleton engineering strategy. Inset images: photographs of the corresponding four Tp COFs.[70] Reproduced with permission from Ref. [70]. Copyright (2020) Chinese Chemical Society.

achieve a high area capacitance of 84 mF cm^{-2} (8.8 F g^{-1}) with the energy and power densities of 2.9 μWh cm^{-2} and 61.8 μW cm^{-2}, respectively.[69]

2.1.3.2. Non-framework structured POPs

Porous materials are functional materials with a pore structure consisting of a continuous solid phase of the material skeleton and a gas or liquid phase that forms pores.[72] POPs are often divided into crystalline porous organic polymers (represented by COF materials) and amorphous porous organic polymers which are a class of highly cross-linked amorphous polymers with nanopores.[73] Typical amorphous porous organic polymers mainly include conjugated microporous polymers (CMPs), porous aromatic backbones (PAFs) and super cross-linked porous polymers (HCPs). Recently, amorphous porous organic polymers with nano-, micron-, or mesoporous structural features have been extensively studied for gas storage and separation, catalysis, and photovoltaic power generation. Also, due to their tunable pore size, large specific surface area and tunable functional groups, they are widely used as active materials for energy storage devices.[13] Herein, we present in detail the application of amorphous porous polymer materials that are not framework-structured in supercapacitors.

Similar to COF materials, incorporating redox-active units into the backbone of these POPs is also a good way to improve its capacitance in supercapacitors. Liao et al. synthesized a three-dimensional polyamineanthraquinone (PAQ) network by coupling 2,6-diamineanthraquinone with aryl bromide via Buchwald-Hartwig (Figure 8). Due to the redox activity of anthraquinone, the PAQs electrode displayed a specific capaci-

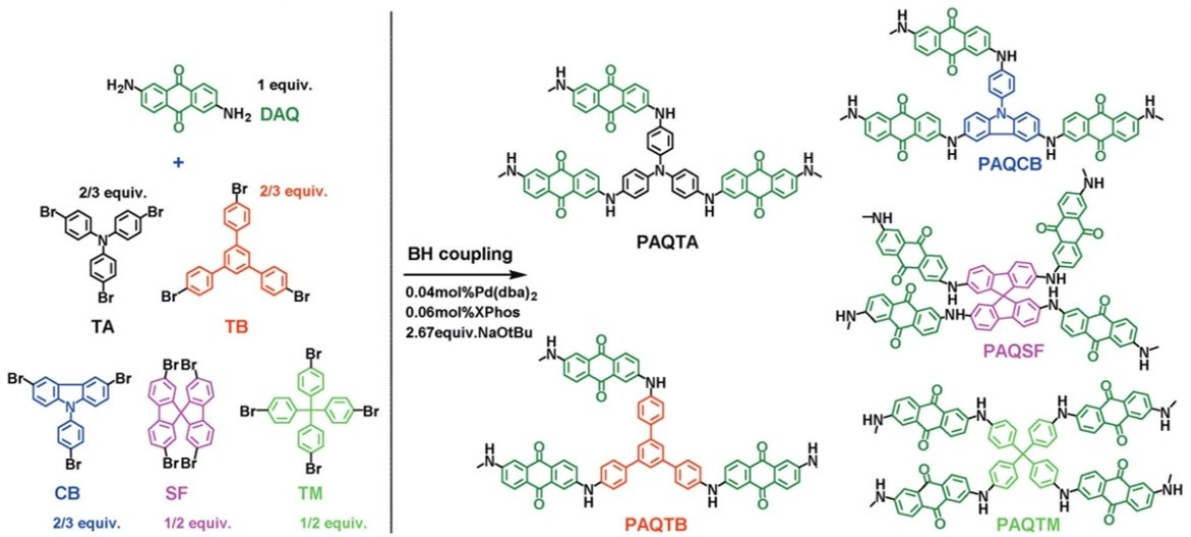

Figure 8. Synthetic route of the PAQs. Reproduced with permission from Ref. [74] Copyright (2018) WILEY-VCH Verlag GmbH & Co. KGaA, Weinheim.

tance of 576 F g^{-1} at 1 A g^{-1} and maintained a capacitance of 80 %–85 % and a coulometric efficiency close to 95 %–98 % after 6000 cycles at 2 A g^{-1}. Furthermore, the asymmetric devices assembled from PAQs exhibited a power density of 1300 W kg^{-1} and an energy density of 60 Wh kg^{-1}.[74]

In addition to carbonyl group in the quinone molecule, redox reactions can also occur on the two carbonyl groups diagonally in the imide moiety. For example, Wakchaure et al. reported a two-dimensional porous polymer derived from hexaaminebenzene and homophthalic dianhydride (Figure 9a). The two-dimensional structure was verified by density function theory. The phthalimide portion of the structure is tilted and arranged to accommodate six units around the benzene ring (Figure 9b). The HOMO of the imide-based POP is located on the benzene ring of the phthalimide (Figure 9c) while the LUMO is located on the imide portion of the polymer (Figure 9d). Due to the redox reaction of the imide functional group (Figure 9e), the polymer charged and discharged at 0.5 A g^{-1} exhibited a specific capacitance of 805 F g^{-1}. After 8000 cycles at 10 A g^{-1}, the capacitance showed only a small decay and remained stable.[75]

2.2. Nitrogen-containing groups

Due to their intrinsic electronegative features and rich precursor sources, nitrogen atoms are widely adopted to modify carbon materials for energy storage application in variety of forms.[80] Indeed, as for supercapacitors with carbon-based electrodes, nitrogen-doping is regarded as one efficient way to enhance their capacitance due to the electronegativity of N compared to C, leading to a migration of electron cloud between them and therefore providing certain pseudocapacitance.[81] In addition, many nitrogen-containing species such as amine groups, nitrogen hetero-derivatives and nitroxyl radicals, etc. can also undergo redox processes to provide pseudocapacitances in supercapacitors, as shown in Figure 10. Among them, nitrogen hetero-derivatives are most commonly investigated. While nitroxyl radical polymers are a class of aliphatic or non-conjugated polymers with radicals as the redox-active center, such as 2,2,6,6-tetramethylpiperidine-nitrogen-oxide (TEMPO). The redox mechanism is a process of insertion of anions into nitroxyl radicals at high reaction potentials and removal of anions at low potentials.[82]

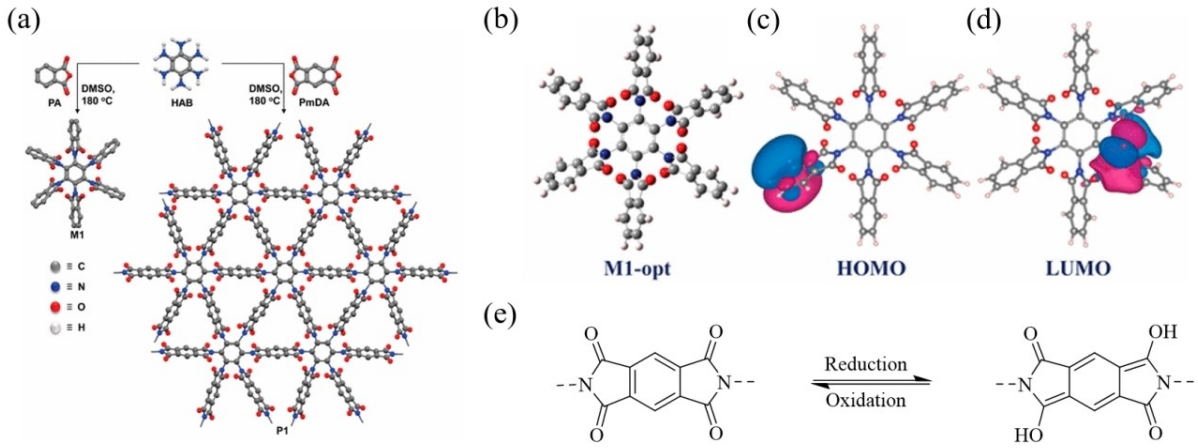

Figure 9. a) Synthetic scheme. b–d) DFT optimized structural model and the corresponding HOMO and LUMO, and e) redox mechanism of the imide-based POP. Reproduced with permission from Ref. [75] Copyright (2020) American Chemical Society.

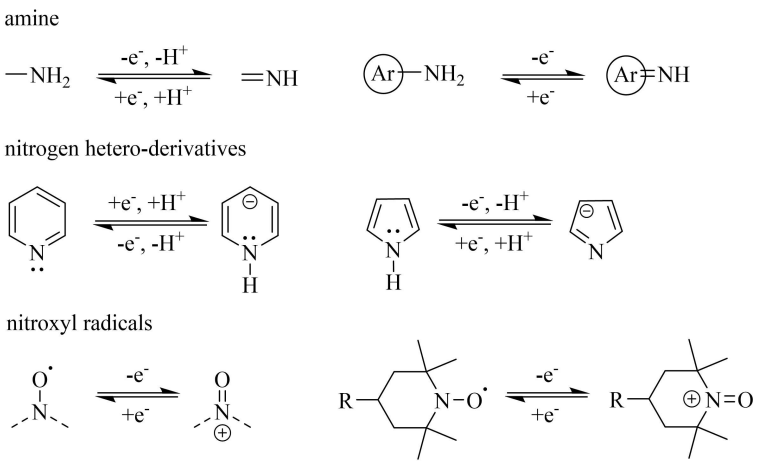

Figure 10. Redox mechanism of nitrogen-containing groups (Ar represents Aromatics).

2.2.1. Small molecules

Among the small molecules, the nitrogen-containing groups involved in redox reactions are mainly $-NH_2$, and its energy storage mechanism is shown in Figure 11. The electrode materials used in supercapacitors are summarized in the following Table 3. Due to their poor electrical conductivity and high solubility in electrolytes, small molecules are often composited with carbon materials through physical or covalent bonding to solve these problems. The physical bonding usually involves interactions such as van der Waals force, hydrogen bonding and electrostatic attraction, which are generally weak. As for the covalent bonding, although many methods such as diazotization and click chemistry, hydrogenation, acylation, and Diels-Alder reaction,[83] have been reported, most of them reduce the electrical conductivity of carbon materials and involve some tedious synthesis steps, leading to additional costs. Therefore, rational design of the structure of the composites to optimize their electrochemical performance is still required.

The most studied amine-based molecule for supercapacitor is p-phenylenediamine (PPD), which is often used with graphene. It can covalently cross-link with graphene and meanwhile is able to intercalate between the layers of graphene to prevent its irreversible re-stacking or agglomeration[84] (Figure 11). Sk et al. covalently functionalized p-phenylenediamine (PPD) with GO nanosheets using the reaction between the two amine groups of PPD and the epoxy and carboxyl groups on the GO substrate. The modified graphene sheet (GPPD) showed a specific capacitance of 282.33 F g^{-1} and an energy density of 39.24 Wh kg^{-1} at a discharge current of 0.75 mA. Additionally, the capacity retention of the material remains approximately 92.82% at a constant current density of 1 mA after 1000 cycles.[85] Lu et al. synthesized rGO composites modified with PPD by a simple solvent method. The final products obtained through two synthesis routes, i.e., modification followed by reduction or reduction followed by modification, were called GPPDH and GHPPD, respectively. Due to the different synthetic routes, the product GPPDH with PPD molecules inserted between graphene sheets showed loose and wrinkled microstructure, while the GHPPD composites have graphene sheets stacked and cross-linked. Consequently, the specific capacitance values of GPPDH and GHPPD at 10 mV s^{-1} were 316.54 and 249.24 F g^{-1} and the capacitance retention was 93.66% (GPPDH) and 87.14% (GHPPD) after 4000 cycles at a current density of 2 A g^{-1}. Moreover, the energy densities of GPPDH and GHPPD supercapacitors were calculated to be 27.01 and 20.53 Wh kg^{-1}, and the specific power densities were 926.06 and 1063.92 W kg^{-1}, respectively.[86] These differences of electrode performances can be mainly explained by the optimized micro-structure of GPPDH compared to that of GHPPD.

In another case, small molecules with different isomeric structure also show different performance as electrode. The higher the E_{HOMO} level of the molecule, the higher pseudocapacitance it will achieve. When they are compounded with carbon materials, the high E_{HOMO} level can reduce the energy barrier between the carbon material and the molecule, ultimately leading to a high capacitance.[87] Zhao et al. compared the pseudocapacitance contributions of two isomeric molecules, 1,5-naphthalenediamine (1,5-NAPD) and 1,8-naphthalenediamine (1,8-NAPD). After compositing with N-doped graphene (NG), the 1,5-NAPD/NG and 1,8-NAPD/NG were used as working electrodes, respectively. CV test showed that the 1,5-NAPD molecule exhibited two redox peaks at 0.1 and 0.3 V, respectively, while the 1,8-NAPD molecule showed only a broad redox peak at 0.35 V (Figure 12a). The Coulomb efficiencies of the symmetric devices assembled with 1,8-NAPD/NG and 1,5-NAPD/NG were calculated to be 95% and 92%, respectively. Besides, the specific capacitance of 1,5-NAPD/NG reached 877 F g^{-1}, which was much higher than that of the 1,8-NAPD/NG film (678 F g^{-1}), as calculated from the GCD curves at 1 A g^{-1}

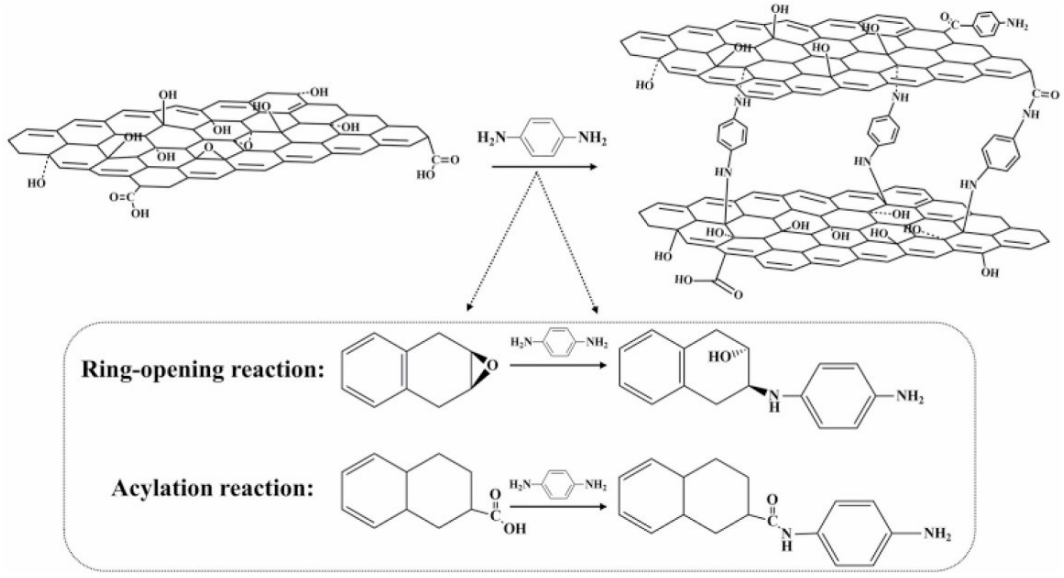

Figure 11. The possible formation mechanism between GO and PPD. Reproduced with permission from Ref. [84] Copyright (2021) Elsevier B.V.

Table 3. Electrode materials based on small molecules with nitrogen-containing groups.

Materials	Preparation	Electrolytes	Specific capacitance, current density	Capacity retention, Cycle number	Energy density [Wh kg^{-1}], power density [W kg^{-1}] (two-electrode)	Electrode system	Ref.
 (TBHQ-GNS)	sonication	1 M H_2SO_4	302 F g^{-1} at 0.25 A g^{-1}	94% (800)	/	three	[90]
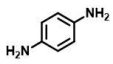 (PPD–C-DCNT)	covalent reaction	1 M H_2SO_4	388 F g^{-1} at 1 A g^{-1}	85.7% (10000)	19.1, 800	three	[91]
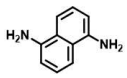 (1,5-NAPD/NG)	post-processing	1 M H_2SO_4	877 F g^{-1} at 10 mV s^{-1}	105% (5000)	/	three	[87]
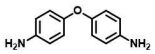 (4,4′-Diphenylamine/NG)	post-processing	2 M Li_2SO_4	630 F g^{-1} at 5 mV s^{-1}	84% (5000)	/	three	[88]
 (MWCNTs-TEMPO)	a two-step reaction	2 M KOH	66 F g^{-1} at 0.25 A g^{-1}	90% (4000)	21.4, 893.4	three	[63]
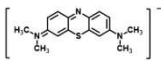	solvothermal method	0.5 M H_2SO_4	517 F g^{-1} at 0.5 A g^{-1}	91% (2000)	30.36, 700	three	[24]
 (HQSA-rGO)	wet chemical method	1 M H_2SO_4	220 C g^{-1} at 0.5 A g^{-1}	99% (10000)	6.25, 522	three	[92]
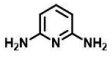 (RGO/DA)	solvothermal method	1 M H_2SO_4	193.51 F g^{-1} at 0.5 A g^{-1}	85.56% (20000)	14.55, 350	two	[93]
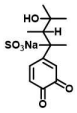 (LS-GH)	hydrothermal	PVA-H_2SO_4	408 F g^{-1} at 1 A g^{-1}	84.4% (10000)	13.8, 500	two	[94]

(Figure 12c). Figure 12(e, f) shows that the E_{HOMO} level of 1,5-NAPD at −5.18 eV is higher than that of 1,8-NAPD at −5.34 eV, further prove that the E_{HOMO} level of different NAPD isomers result in different pseudocapacitance contribution.[87] In addition, small aromatics containing amino groups usually display better cycling properties compared to those containing both hydroxyl and amino groups. This may be due to the fact that the redox of molecules without –OH involves a greater energy change, which in turn yields a better cyclic stability.[87] The same research group also selected eight amino-containing molecules ((4-aminephenol (AP), 2-AP, 1,5-naphthalenediamine (NAPD), 1,8-NAPD, 4,4′-oxydianiline (ODA), 3,4′-ODA, 4,4′-thiodianiline (TDA), and 2,2′-TDA)) to functionalize N-doped graphene and compared the electrochemical properties of these composites. The graphene films compounded with 1,5-NAPD showed the highest specific capacitance and achieved 105% capacitance retention after 5000 cycles. The maximum energy density of the symmetric device based on 1,5-NAPD/NG films achieved 31 kWh kg^{-1}.[87] The superior electrochemical properties of 1,5-NAPD compared to its counterparts can be mainly attributed to its higher E_{HOMO} level and large energy changes in redox processes.

To gain insight into the effects of functional groups and molecular structure on the pseudocapacitive behavior of aromatic molecules, Zhao et al. also functionalized NG films with four different types of aromatic molecules (4,4′-oxydiphenol, 4,4′-oxydianiline, 3,3′-dihydroxydiphenylamine; and diaminebenzidine) via a simple post-processing process and compared their electrochemical properties. Among the selected organic compounds, the 4,4′-oxydianiline molecule was ob-

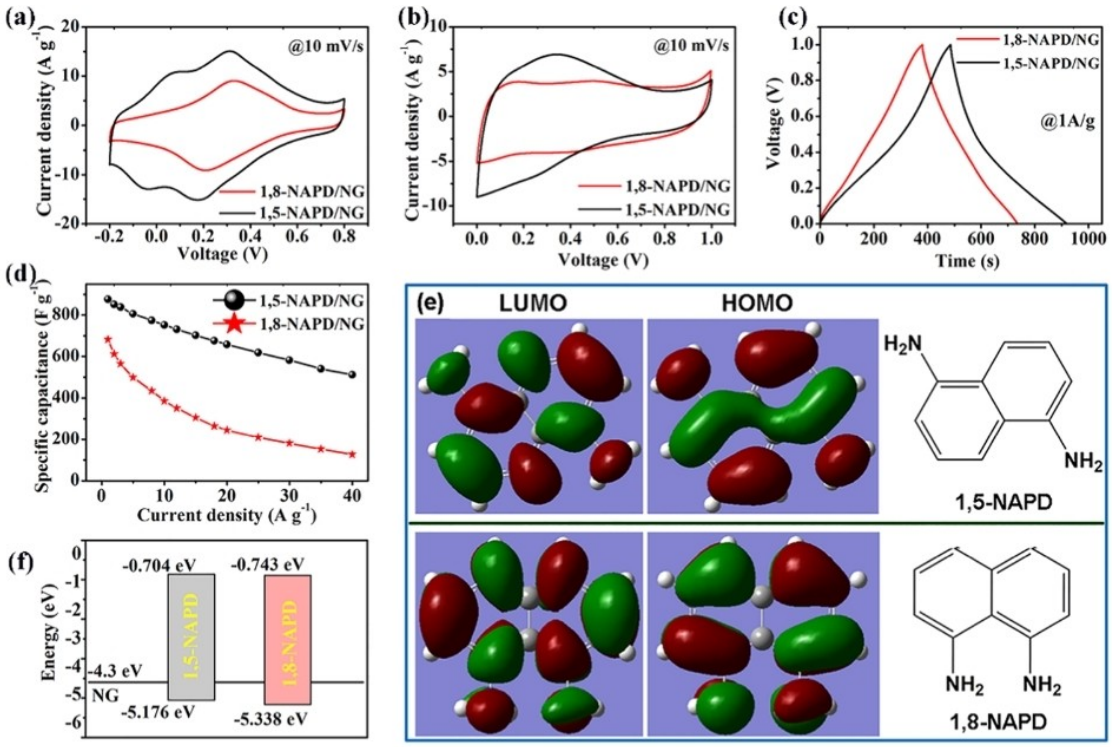

Figure 12. a) CV loops at 10 mV s^{-1} collected from a three-electrode system using 1,5-NAPD/NG and 1,8-NAPD/NG as work electrodes, respectively. Using a two-electrode symmetric configuration, CV loops corresponding to NAPD/NG and 1,8-NAPD/NG films are shown in b). c) GCD curves collected from symmetric cells based on NAPD/NG and 1,8-NAPD/NG films, respectively. d) Specific capacitances of the two electrode films at various current densities. e) Frontier MO diagrams of 1,5-NAPD and 1,8-NAPD molecules. f) Energy-level diagram. Reproduced with permission from Ref. [87] Copyright (2019) American Chemical Society.

served to have superior electrochemical properties in Li_2SO_4 electrolyte. Upon a scan rate of 5 mV s^{-1}, the 4,4′-oxydianiline/NG sample showed the highest capacitance value of 630 F g^{-1} and 84% of capacitance retention after 5000 cycles,[88] and maintained a high coulombic efficiency within a voltage window of 1.6 V. Through the comparison of molecular structures and electrochemical properties of the four molecules, it was found that the aromatic molecules containing –OH groups exhibit stronger adsorption affinity for NG lamellae than those contain only $–NH_2$. Besides, a single molecule containing more redox-active groups does not mean that it can provide higher pseudocapacitance. Moreover, the cycling stability and the ability to maintain a wider voltage window of molecules with $–NH_2$ groups are superior to those with –OH groups in Li_2SO_4 electrolyte.

Note that there are also organic molecules containing amino groups that were used as electrodes in supercapacitors but their pseudocapacitive characteristics were not mentioned.[39,89] This observation is suspected mainly due to the following factors: First, the voltage window adopted for the electrode molecules is not sufficient to activate the amino groups to undergo a reversible redox reaction; Second, the electrode molecules are not electrically conductive to stimulate the pseudocapacitive characteristics of the amino groups. Indeed, amino groups can undergo redox reactions to provide pseudocapacitance if they are conjugated well in the molecular structures, as evidenced in conducting polymers such as polyaniline.

2.2.2. Linear-structured polymers

In the past decades, nitrogen-containing linear polymer molecules, such as polypyrrole, polyaniline, polycarbazole,[95,96] poly(ortho-aminephenol),[97–99] and poly(phenylenediamine),[100–104] have been extensively studied. Compared with the other nitrogen-containing linear polymers that are not conjugated, nitrogen-containing conducting polymers such as polypyrrole and polyaniline have the advantages of good electrical conductivity and electrochemical activity, high theoretical capacitance and easy synthesis, and therefore become representative organic electrode materials for the development of high-performance supercapacitors.[105] Herein, we mainly summarize these two conducting linear polymers with nitrogen-functionality and describe their energy storage mechanisms below.

2.2.2.1. Polypyrrole

PPy is a typical p-doped conducting polymer with a maximum doping level of 0.33, and its energy storage mechanism is

shown in Figure 13.[15] In recent years, PPy is one of the most widely studied polymeric materials used to fabricate electrodes due to its unique properties such as high electrical conductivity, fast charging/discharging processes, ease of synthesis, good flexibility, and cost-effectiveness.[106]

Back to 1996, Clemente et al. prepared a conducting polymer electrode via a constant-current polymerization method and assembled a fully polymerized redox supercapacitor based on polypyrrole negative electrode and polyaniline positive electrode using a polymethyl methacrylate (PMMA) membrane as an electrolyte separator. The solid-state device can obtain specific energy of 4 Wh kg^{-1}, a specific power of 1000 W kg^{-1}, and provide up to 60% of full capacitance in several thousand charge/discharge cycles.[107]

PPy has a high theoretical specific capacitance of 620 F g^{-1}, while the actual specific capacitance falls far short of this value. Various scientific efforts have been paid to enhance its capacitance.

By optimizing the morphological structure of PPy, its electrochemical properties can be improved.[15] Dubal et al. synthesized one-dimensional PPy nanotubes (PPy–NTs) using anionic azo dye methyl orange (MO) via a chemical oxidation-mediated soft-template oriented route. The PPy–NTs showed a capacitance of more than 332 F g^{-1} in 1 M H_2SO_4.[108] In another report, Zhao et al. synthesized PPy nanowires by chemical oxidative polymerization under mild conditions using iron trichloride as the oxidant. Nano-gaps or pores were formed in the PPy nanowires due to their intertwined nanostructures. The resulting electrodes obtained a specific capacitance of 420 F g^{-1} at 1.5 A g^{-1} and maintained 97.9% of the initial capacitance after 8000 cycles.[109] Wang et al. prepared 3D porous PPy films by adopting a porous template ($CaCO_3$) via a modified gas-phase polymerization method. The optimized 3D porous PPy film electrode provided a high capacitance of 313.6 F g^{-1} at 1.0 A g^{-1} in a three-electrode configuration, and high capacitance retention of up to 81.3% was obtained after 10,000 GCD cycles. The porous structure provides PPy films with the adapting capability to volume changes during doping/de-doping, which is critical to maintain a long cycle life in supercapacitors.[110]

The selection of suitable molecular doping can also be used to improve the electrochemical properties of PPy. Wang et al. described for the first time a general supramolecular approach for the in-situ synthesis of one-dimensional nanostructured PPy conductive hydrogels using an anti-balance ion (a disc-shaped liquid crystal molecule copper phthalocyanine) as dopant. The dopant 3,4′,4″,4‴-tetrasulfonic acid tetrasodium salts (CuPcTs) crosslinked PPy chains to form 3D network hydrogels with a homogeneous morphology of interconnected nanofibers. Moreover, the specific capacitance of CuPcTs-doped PPy at 0.2 A g^{-1} is ~ 400 F g^{-1}, while that of the pristine PPy is only 232 F g^{-1}. The better performance of CuPcTs-doped PPy can be attributed to the enhanced charge transportation crossing the CuPcTs-doped PPy chains.[111] Note that some of the dopants can also undergo redox reactions during the charging/discharging process to provide additional capacitance to the electrodes. Zhang et al. synthesized PPy doped with heptamolybdate anion ($Mo_7O_{24}^{6-}$) by electro-polymerization. The as-prepared material exhibited a stem-like morphology. The poly counter ions with large spatial site resistance can be used as structural columns to give PPy an open structure for ion transport. In addition, $Mo_7O_{24}^{6-}$ also provided part of the redox activity. The PPy electrode with thickness of ~2 mm and a mass loading of 192 mg cm^{-2} finally reached a surface capacitance of 47 F cm^{-2} at 2 mA cm^{-2}. The obtained symmetrical supercapacitor assembled in a 3 M LiCl electrolyte displayed an area capacitance of 12.4 F cm^{-2} at 1 mA cm^{-2} and provided a good area energy density of 2.48 mWh cm^{-2} at a power density of 0.619 mW cm^{-2}. Moreover, the capacitance retention rate was 96.4% after 5000 charge/discharge cycles.[112]

In addition to the structural design of PPy itself, a large number of studies have also been conducted to combine it with carbon/other pseudocapacitive materials (Table 4) to obtain binary/ternary composites and achieve improved electrochemical performance in supercapacitors.

2.2.2.2. Polyaniline

As another typical conductive polymer, polyaniline owns three main stable oxidation states: half-oxidized emeraldine base (EB), fully oxidized pernigraniline (PE) and fully reduced leucoemeraldine (LE).[131] Different redox forms of polyaniline store charges when switching between multiple oxidation states through redox processes[132] (Figure 14). For a single PANI electrode, the maximum theoretical capacitance is 2000 F g^{-1}, much higher than other conducting polymers.[133]

In 1993, Huang et al. first used PANI as an electroactive material for supercapacitors. The specific capacitance of the flat capacitors can achieve approximately more than 100 pF. In 2001, Fusalba et al. prepared electroactive PANI films on carbon paper electrodes in non-aqueous solutions using an organic acid (CF_3COOH) as a proton source. The capacitance was measured to be 150 F g^{-1} in a three-electrode system. The PANI-based symmetric supercapacitor showed a discharge capacity loss of about 60% after 1000 cycles in a non-aqueous medium. Moreover, using tetramethylammonium methanesulfonate ($Me_4NCF_3SO_3$) as the supporting electrolyte in acetonitrile, the assembled supercapacitors showed an energy density of 3.5 Wh kg^{-1} and a power density of 1300 W kg^{-1}.[134]

The nanostructure of PANI has obvious impact on their electrochemical properties since it influences the ionic accessibility to the redox sites.[15] Therefore, it is essential to develop

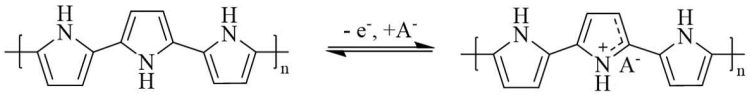

Figure 13. Energy storage mechanism of PPy.

Table 4. Electrode materials based on PPy.

Materials	Preparation method	Electrolytes	Specific capacitance, current density	Capacity retention, Cycle number	Energy density [Wh kg^{-1}], power density [W kg^{-1}] (two-electrode)	Electrode system	Ref.
PPy-NTs	chemical oxidation-mediated soft templating	1 M H_2SO_4	332 F g^{-1} at 1 mA cm^{-1}	89.98 % (2000)	28.95, 7750	three	[108]
CNF-PPy/PB	*in situ* oxidative polymerization	6 M KOH	236.9 F g^{-1} at 0.5 A g^{-1}	86.0 % (1500)	/	three	[113]
ECNT/PPy	electrochemical deposition	5 M LiCl	965.3 mF cm^{-2} at 1 mA cm^{-2}	89.1 % (10000)	3.63 mWh cm^{-3}, 13.86 mW cm^{-3}	three	[114]
GPs-1WNTs/PPy	*in situ* polymerization	1 M H_2SO_4	1224 F g^{-1} at 0.5 A g^{-1}	84 % (5000)	28.8, 1975.22	three	[115]
PPy@rGOH	hydrothermal synthesis process, *in situ* electropolymerization	1 M KNO_3	340 F g^{-1} at 1 A g^{-1}	87.4 % (10000)	46.9, 800	three	[116]
SDBSDPPy HC	emulsion polymerization	6 M KOH	1086 F g^{-1} at 5 mV s^{-1}	90 % (2500)	/	three	[117]
$NiCo_2O_4$/rGO/PPy	hydrothermal synthesis and *in situ* polymerization	1 M KOH	1547 ± 5 F g^{-1} at 0.5 A g^{-1}	94 ± 1 % (5000)	34.37 ± 0.11, 99.98 ± 0.31	three	[118]
PPy/PANI@-MoS_2	*In situ* polymerization methods	1 M H_2SO_4	1171 F g^{-1} at 1 A g^{-1}	99.2 % (10000)	93.4, 884,8	three	[119]
PPy/LWCA	sol-gel techniques	6 M KOH	421.45 F g^{-1} at 1 A g^{-1}	82.9 % (5000)	52, 2012.8	three	[120]
PPy/C_3N_4	electrochemical deposition	0.1 M $LiClO_4$	810 F g^{-1} at 0.2 A g^{-1}	92 % (6000)	/	three	[121]
$CeVO_4$/PPy	hydrothermal	1 M KOH	116 F g^{-1} at 0.75 A g^{-1}	77.80 % (10000)	52.2, 675.9	two	[122]
PPy-G–Ni-W	*in situ* polymerization method	1 M Na_2SO_4	342 F g^{-1} at 0.5 A g^{-1}	96.4 % (5000)	14.4, 275	two	[123]
PPy/PA	one-pot fabrication step	2 M KOH	205.5 F g^{-1} at 1 A g^{-1}	84 % (5000)	44.8, 850	two	[124]
PPy film	a modified vapor phase polymerization	1 M Na_2SO_4	62.5 F g^{-1} at 0.5 A g^{-1}	81.3 % (10000)	/	two	[110]
Ni_3S_2@PPy/NF	a facile hydrothermal followed by electrodeposition method	PVA-KOH	425 mF cm^{-2} at 2.0 mA cm^{-2}	87.7 % (2000)	46.4, 166.7	two	[125]
PPy/Ni_3S_2	hydrothermal method, electrodeposition method	3 M KOH	93.6 C g^{-1} at 0.5 A g^{-1}	91.7 % (10000)	74.9, 1356.4	two	[126]
PMo_{12}/PPyNT	hard template assist	1 M H_2SO_4	132.5 F g^{-1} at 2.9 A g^{-1}	73.2 % (5000)	36.1, 6660	two	[127]
PPy g-1O/ARS	a facile one-step hydrothermal method	1 M H_2SO_4	134 F g^{-1} at 15 A g^{-1}	84.4 % (10000)	60.3, 900.7	two	[128]
PPy/KCSF/Ag	*in situ* polymerization method	PVA/LiCl	978.9 mF cm^{-2} at 1 mA cm^{-2}	80 % (2000)	80.3, 0.38	two	[129]
PPy jute fabrics	electrochemical polymerization	0.1 M H_2SO_4	39.9 F g^{-1} at 1 A g^{-1}	/	250 μWh cm^{-2}, 1100 μW cm^{-2}	two	[130]
PPy-Mo_7O_{24}	electropolymerization	3 M LiCl	12.4 F cm^{-2} at 1 mA cm^{-2}	96.4 % (5000)	2.48 mWh cm^{-2}, 0.619 mW cm^{-2}	two	[112]

facile synthetic methods to prepare PANI with suitable nanostructures. Tan et al. successfully prepared hollow PANI microspheres (HMsPANI) using sulfonated polystyrene microspheres as template. The prepared electrode consisted of nanoparticles and had a layered structure. A maximum specific capacitance of 421 F g^{-1} was achieved in 1 M H_2SO_4.[135] Dhawale et al. synthesized nanostructured PANI electrodes by a one-step template-free and seedless method. The specific capacitance reached a maximum value of 503 F g^{-1} at 1 mA cm^{-2} and the specific energy and power densities were 96.23 Wh kg^{-1} and 8.88 kW kg^{-1}, respectively.[136] Wang et al. reported a template-free approach to synthesize large arrays of vertically aligned PANI nanowires on various conducting substrates using a galvanostatic current method. The prepared large arrays of PANI nanowires had narrow diameters and were oriented perpendicular to the substrate, which was believed to facilitate the ion diffusion process when used as supercapacitor electrodes. Consequently, the PANI nanowire exhibited outstanding elec-

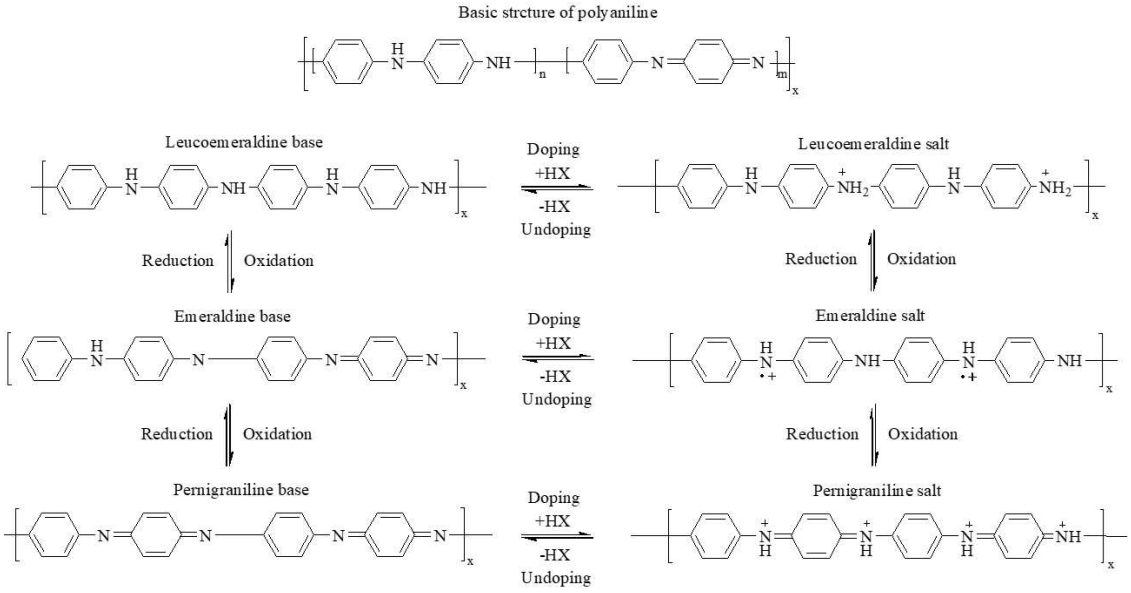

Figure 14. Energy storage mechanism of different redox forms of polyaniline. Reproduced with permission from Ref. [132] Copyright (2021) Elsevier Ltd.

trochemical performance with a specific capacitance up to 950 $F g^{-1}$ at 1 $A g^{-1}$ and an initial capacitance retaining 88% after 500 loops at 20 $A g^{-1}$ in 1 M $HClO_4$ aqueous solution.[137]

Similar to that of PPy, properly doping PANI with dopants can also optimize its electrochemical properties. In 2002, Ryu et al. compared the effect of dopants, namely HCl or $LiPF_6$ on the performance of the fabricated symmetrical supercapacitors with $EtNBF_4$ as the electrolyte. PANI-$LiPF_6$ exhibited an initial capacity of ~107 $F g^{-1}$ and a capacitance of ~84 $F g^{-1}$ after 9000 cycles, while PANI-HCl electrodes showed a capacitance of 40 $F g^{-1}$ after 400 cycles.[138] Since lithium salt-doped PANI is easily oxidized and reduced electrochemically, it achieved a larger discharge specific capacitance than the protonate-doped PANI. Wu et al. selected several organic acids, i.e., malic acid (MA), propionic acid (PA), succinic acid (SA), tartaric acid (TA) and citric acid (CA), etc. as dopants for the synthesis of homogeneous PANI nanotubes via a facile chemical soft template method. As MA has two hydrophilic COOH ending groups, it provides both doping property and hydrogen bonding interaction during the polymerization of aniline, which optimizes the structure of the obtained PANI and thus improves its electrochemical properties. Consequently, the PANI-MA nanotubes displayed the highest specific capacitance of 658 $F g^{-1}$ at 0.1 $A g^{-1}$ in 1 M H_2SO_4 electrolyte. After 1200 charge/discharge cycles at 100 $mV s^{-1}$, the PANI-MA electrodes still retained 64.0% of its initial specific capacitance.[139]

Nevertheless, as a supercapacitor electrode material, the application of PANI is still limited by its low practical capacitance and poor cycling stability. Therefore, combination of PANI with highly conducting and other pseudocapacitive materials, to fabricate PANI-based electrodes with enhanced cycling stability and capacitance, is widely investigated and reported (Table 5).

2.2.3. Porous organic polymers (POPs)

2.2.3.1. Framework structured POPs-COFs

In principle, the presence of nitrogen heteroatoms can provide a certain pseudocapacitance for the COF-based electrode material, which originates from the Faraday reaction caused by the interaction of the lone pair of electrons of N with the electrolyte cation (e.g., H^+).[160] Furthermore, the presence of heteroatoms (N, P, S, etc.) can also help enhance electron density, improve the exposed area, boost the ion diffusion rate, and hence benefit for the supercapacitor performance.[161] Table 6 summarizes the application of COFs containing nitrogen functional groups that are used as electrode material in supercapacitors. Among all, triazine group is one representative that can participate in redox reactions.[78,162] Xue et al. designed a microporous phosphonitrile-triazine COF (HM-COF) (Figure 15a) prepared using hexachlorocyclotriphosphonitrile (HCCP) and melamine (MA) as precursor materials. The maximum specific capacitance of HM-COF was 145 $F g^{-1}$ at 0.5 $A g^{-1}$ due to the redox reactions occur on the triazine groups. The capacitance retention kept 84.6% of the initial capacitance after 30,000 cycles.[163] Li et al. synthesized DBT-MA-COF (Figure 15b) by carbon-nitrogen coupling reaction using 2,5-dibromothiophene (DBT) and melamine (MA) as monomers. The energy storage mechanism corresponds to the quasi-reversible redox process of the triazine units (Figure 15c). The assembled asymmetric supercapacitor DBT-MA-COF//C–CTS ASC showed a high energy density of 32.1 Wh kg^{-1} and a power density of 800 W kg^{-1}. Besides, an initial capacitance retention rate of 83% was achieved after 30,000 consecutive constant current charge/discharge cycles.[78]

In addition to triazine, some other nitrogen-containing groups such as imine, carbazole and pyridine can also provide pseudocapacitance. EL-Mahdy et al. prepared three new β-

Table 5. Electrode materials based on PANI.

Materials	Preparation method	Electrolytes	Specific capacitance, current density	Capacity retention, Cycle number	Energy density [Wh kg^{-1}], power density [W kg^{-1}] (two-electrode)	Electrode system	Ref.
PANI	one-step without template method, constant current method	1 M $HClO_4$	950 F g^{-1} at 1 A g^{-1}	88% (500)	/	three	[137]
PANI	one-step template-free seedless growth of nanostructures	1 M H_2SO_4	503 F g^{-1} at 1 mA cm^{-2}	very small decrease (10000)	96.23, 8800	three	[136]
SGN/PANI	interface aggregation	1 M H_2SO_4	497 F g^{-1} at 0.2 A g^{-1}	94.3% (2000)	/	three	[140]
RGO-PANI	*in situ* polymerization	1 M H_2SO_4	361 F g^{-1} at 0.3 A g^{-1}	82% (1000)	/	three	[141]
$Ti_3C_2T_x$@PANI-RGO	a low-temperature hydrothermal	1 M H_2SO_4	617.84 F g^{-1} at 0.5 A g^{-1}	92.52% (10000) (two-electrode)	269.18, 527.72	three	[142]
MXene-Ti_2CT_x@PANI	*in situ* polymerization	0.5 M KOH	635 F g^{-1} at 1 A g^{-1}	97.54% (10000)	42.3, 950	three	[143]
PANI@CNF-PVA	*in situ* oxidative polymerization	1 M H_2SO_4	226.1 F g^{-1} at 0.2 A g^{-1}	74% (3000)	/	three	[144]
PANI/$Ti_3C_2T_x$	a facile and cost-effective self-assembly	1 M H_2SO_4	462 F g^{-1} at 1 A g^{-1}	84.5% (5000)	50.8, 900	three	[145]
SPANI-ABF-G	chemical polymerization and molecular self-assembly	1 M H_2SO_4	642.6 F g^{-1} at 1 A g^{-1}	100% (5000)	/	three	[146]
PANI-g-CF	chemical oxidative polymerisation	1 M H_2SO_4	441 F g^{-1} at 1 A g^{-1}	88.80% (10000)	/	three	[147]
CNT g-1/PANI	*in situ* polymerization	1 M H_3PO_4	261.5 mF cm^{-2} at 0.1 mA	80% (5000)	36.3–29.4 μWh cm^{-2}, 0.17–5 mW cm^{-2}	two	[148]
PANI/ACTBs	*in situ* polymerization	1 M H_2SO_4	154 F g^{-1} at 1 A g^{-1}	86% (10000)	42,699	two	[149]
PANI/RGO	physical mixing	1 M H_2SO_4	112 F g^{-1} at 0.08 A g^{-1}	86% (17000)	8.80 mWh cm^{-3}, 30.77 mW cm^{-3}	two	[150]
PVA-PANI	*in situ* polymerization	PVA-PA	260.1 mF cm^{-2} at 0.5 mA cm^{-2}	97.5% (1000)	14.3 Wh cm^{-2}, 97.5 W cm^{-2}	two	[151]
APH-PANI	freeze-thaw method, directional freezing method	PVA-H_2SO_4	25.86 mF cm^{-2} at 0.05 mA cm^{-2}	94% (2000)	/	two	[152]
PANI@paper	a facile mechanically enhanced polymerization method	1 M H_2SO_4	296 F g^{-1} at 1 A g^{-1}	86.1% (1000)	2.5, 300	two	[153]
Ti@PEDOT-PANi	a potentiostatic method	1 M H_2SO_4	2876 mF cm^{-2} at 5 mA cm^{-2} (three-electrode)	72.1% (5000)	15.9 mWh cm^{-3}, 178.9 mW cm^{-3}	two	[154]
Layered HPC/PANI	*in situ* oxidative polymerization	1 M Na_2SO_4	643 F g^{-1} at 1.0 A g^{-1} (three-electrode)	88.0% (5000)	36.3, 850.2	two	[155]
RGO/CMC-PANI	*in situ* oxidative polymerization	1 M H_2SO_4	81.8 F g^{-1} at 1 mA cm^{-2}	87.3% (20000)	140.6 μWh cm^{-2}, 749.9 μW cm^{-2}	two	[156]
OA PANi	seed polymerization	1 M H_2SO_4	343.8 F g^{-1} at 2 A g^{-1}	82.8% (5000)	30, 601.7	two	[157]
PANI@Au@CNT	thermal evaporation and electrochemical deposition	1 M H_2SO_4	6 F cm^{-3} at 10 V s^{-1}	94.5% (5000)	/	two	[158]
ACF-PANI	electrochemical and chemical methods	0.5 M H_2SO_4	61 F g^{-1} at 500 mA g^{-1}	90% (1000)	20, 2100	two	[159]

ketenamine-linked COFs by condensation of homotrisalicylaldehyde (TFP-3OHCHO) with comonomers of tris(aminephenyl) derivatives-amine, carbazole or pyridine via Schiff base [3 + 3] (Figure 16). The prepared TFP-COFs exhibited an electrochemical specific capacitance of 291.1 F g^{-1} at 2 A g^{-1} due to the presence of the redox-active N-containing groups, and were able to maintain 91% of the initial capacitance for 5000 cycles at 10 A g^{-1}.[164]

Table 6. Electrode materials based on framework-structured polymers containing nitrogen functional groups.

Materials	Preparation	Specific capacitance, current density	Capacity retention, Cycle number	Energy density [Wh kg^{-1}], power density [W kg^{-1}] (two-electrode)	Electrode system	Ref.
CNT@TFA-COF	a facile one-pot method	338 F g^{-1} at 1 A g^{-1}	86% (7000, 5 A g^{-1})	/	three	[168]
COP-2	solvothermal heating condition	404 F g^{-1} at 0.5 A g^{-1}	100% (50000)	14, 1848	three	[169]
Tp-AT-POP	solvothermal Schiff-base condensation	348.3 F g^{-1} at 0.5 A g^{-1}	71% (5000)	26.02, 2120	three	[170]
HM-COF	solvothermal reaction	145 F g^{-1} at 0.5 A g^{-1}	84.6% (30000, 2 A g^{-1})	/	three	[163]
DBT-MA-COF	solvothermal reaction	407 F g^{-1} at 1 A g^{-1}	85% (20000, 5 A g^{-1})	32.1, 800	three	[78]
TAPT-2,3-NA(OH)$_2$	Schiff-base polycondensations	271 F g^{-1} at 0.5 A g^{-1}	79.1% (5000, 10 A g^{-1})	/	three	[71]
TFP-COFs	Schiff-base polycondensations	291.1 F g^{-1} at 2 A g^{-1}	91% (5000, 10 A g^{-1})	/	three	[164]
CPP	solvothermal method	571 F g^{-1} at 1 A g^{-1}	80% (9000, 6 A g^{-1})	15.4, 292	three	[171]
GT-POP-1	acid catalysis	324 F g^{-1} at 0.5 A g^{-1}	71.2% (10000, 2 A g^{-1}, two-electrode)	24.5, 193	three	[172]
PyBDA	Buchwald-Hartwig coupling	456 F g^{-1} at 0.5 A g^{-1}	130% (5000, 100 mV s^{-1})	/	three	[165]
TpDAB	Schiff-base polycondensation	432 F g^{-1} at 0.5 A g^{-1}	93% (1000, 10 A g^{-1})	60, 7.5	three	[173]
DAB-COF	Schiff base reaction	129.2 F g^{-1} at 0.5 A g^{-1}	100% (20000, 10 A g^{-1})	4.47, 125	three	[174]
2D 250-HADQ COF	a condensation process	516.4 F g^{-1} at 0.5 A g^{-1}	81% (100000, 2 A g^{-1})	219.4, 437.5	two	[175]
ABA-COF	imine condensation reaction	927.9 F cm^{-3} at 10 mV s^{-1}	97% (5000)	/	two	[176]
Tptp-Cof Tpda-Cof	Schiff-base polycondensations	56.4 F g^{-1} at 5 mV s^{-1} 70.6 F g^{-1} at 5 mV s^{-1}	78.60% (10000) 81.54% (10000)	/	two	[177]
PDC-MA-COF	Schiff-base polycondensations	94 F g^{-1} at 1 A g^{-1}	88% (20000, 5 A g^{-1})	29.2, 750	two	[162]

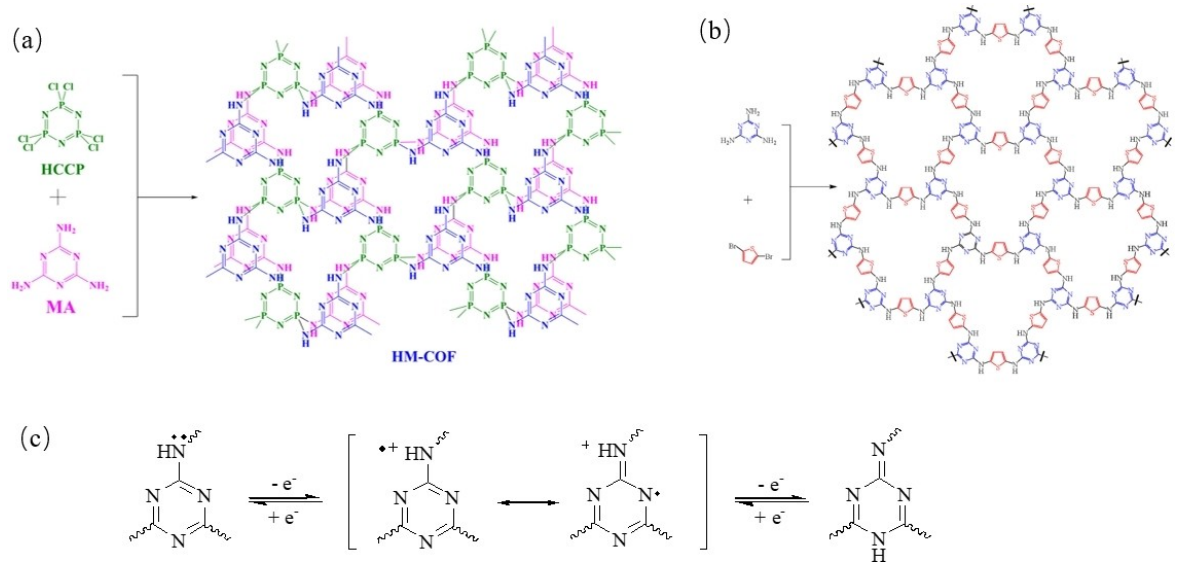

Figure 15. a) Reaction of HCCP and MA. b) Synthesis of DBT-MA-COF. c) Redox transformation of triazine units. Reproduced with permission from Ref. [163] Copyright (2021) Elsevier B.V. Reproduced with permission from Ref. [78]. Copyright (2020) Elsevier Inc.

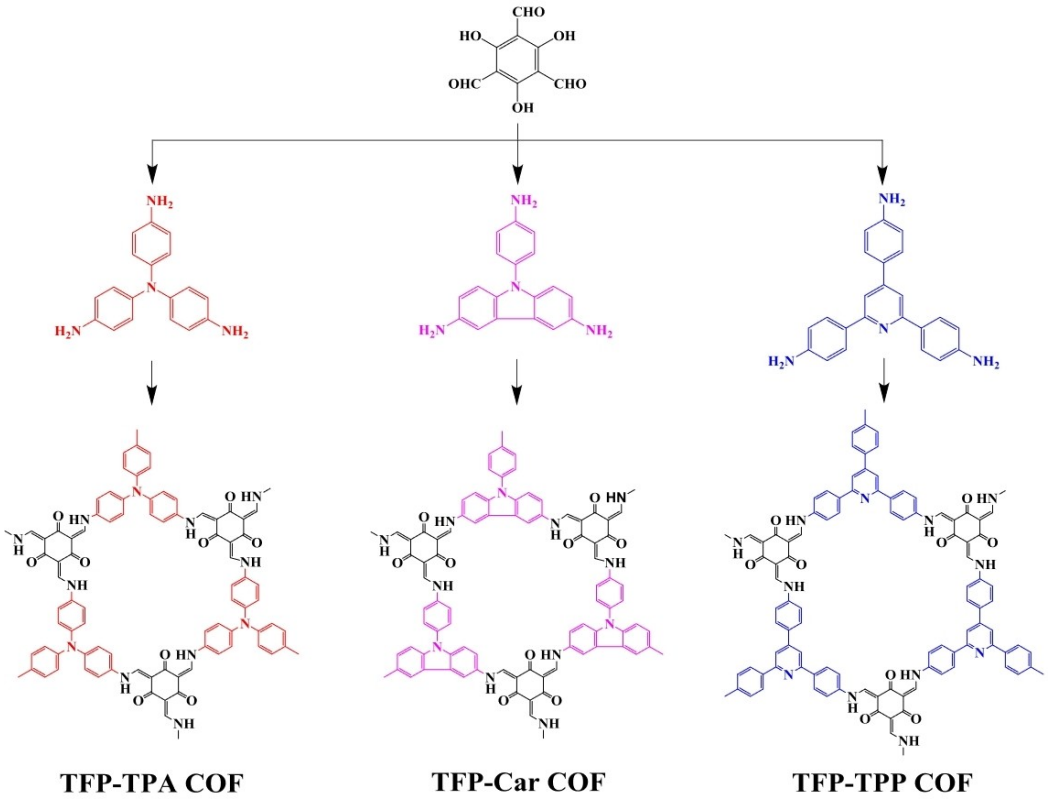

Figure 16. Synthesis of three β-ketoenamine-linked COFs – the TFP-TPA, TFP-Car, and TFP-TPP COFs – from TFP-3OHCHO and tris(aminephenyl) derivatives having different degrees of planarity. Reproduced with permission from Ref. [164] Copyright (2019) Taiwan Institute of Chemical Engineers.

2.2.3.2. Non-framework structured POPs

Similar to COF, other POPs that are not framework-structured can also provide pseudocapacitance in supercapacitors if they contain groups that can undergo redox reactions. Bandyopadhyay et al. developed a new class of pyrene-based conjugated porous organic polymers with N-containing groups through Buchwald-Hartwig coupling (Figure 17a). The obtained POP

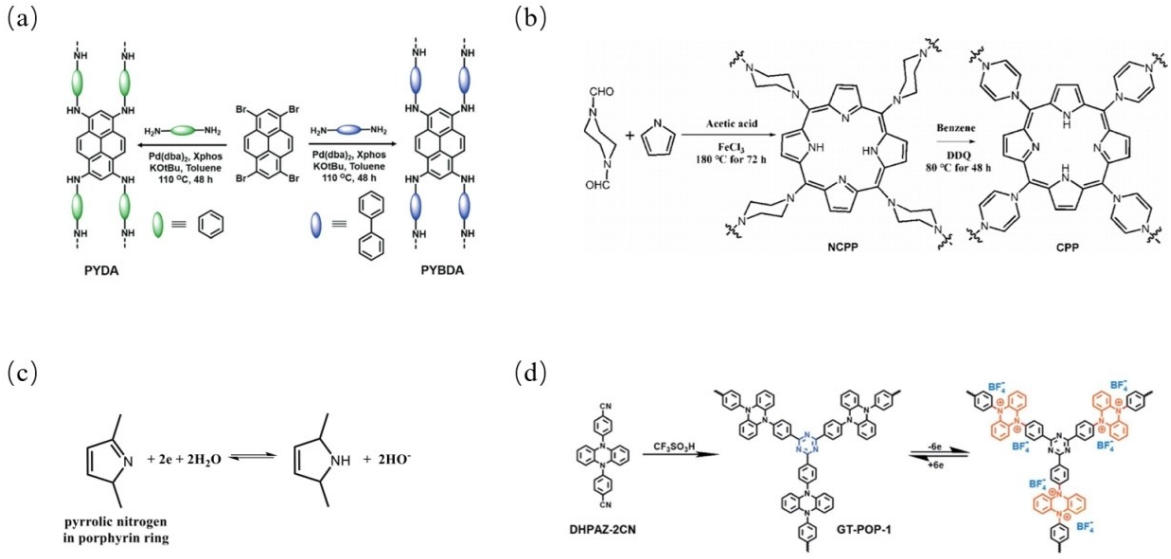

Figure 17. Synthesis of a) PYDA and PYBDA. Adapted from Ref. [165] Copyright (2018) Royal Society of Chemistry. b) Synthesis of CPP. Adapted from Ref. [166] Copyright (2020) Elsevier Ltd. c) Redox mechanism of GT-POP. d) Synthesis and Redox mechanism of GT-POP. Adapted from Ref. [167] Copyright (2020) Royal Society of Chemistry.

with amino groups exhibited a high specific capacitance of 456 $F g^{-1}$ at 0.5 $A g^{-1}$. A capacitance retention of 100% after 2000 cycles was obtained with the capacitance slowly increased to 130% after 5000 cycles.[165] Zhang et al. prepared fully conjugated porphyrin polymers (CPPs) by simple dehydrogenation of region-conjugated polymers (NCPPs) using a solvothermal method (Figure 17b). The obtained CPPs displayed an amorphous structure and nanosheet morphology with abundant pores. Owing to the presence of abundant porphyrin groups with redox activities (Figure 17c) in the backbone, the CPPs electrode achieved a high specific capacitance of 571 $F g^{-1}$ at 1 $A g^{-1}$. An energy density of 15.4 $Wh kg^{-1}$ at a specific power density of 292 $W kg^{-1}$ was obtained and the capacitance retention was maintained at 80% after 9000 cycles at 6 $A g^{-1}$.[166] Zhang et al. synthesized a novel dihydrophenylhydrazine-derived porous organic polymer GT-POP-1 using triflic acid (TfOH) as the catalyst and DHPAZ-2CN as the cyclic trimer. The covalent triazine linkage minimizes the molecular weight of the inactive groups and facilitates the construction of rigid and porous structures. The redox-active 5,10-diphenyl-5,10-dihydrophenanthrene core can undergo two stepwise redox processes (Figure 17d), which in turn leads to an excellent specific capacitance (324 $F g^{-1}$ at 0.5 $A g^{-1}$ for the GT-POP-1 electrode). Furthermore, the specific capacitance of the assembled GT-POP-1//AC device was maintained at 67% after 5000 cycles, and the maximum energy density was 24.5 $Wh kg^{-1}$ at a power density of 193 $W kg^{-1}$.[167]

2.2.3.3. Framework structured POPs-MOFs

Metal-organic frameworks (MOFs) are a class of POPs formed by self-assembly of metal ions and organic ligands through coordination bonding. Due to their high specific surface area, regular pore structure, and highly tunable structural composition, MOFs and their derivatives show great potentials and are widely investigated in gas storage, adsorption and separation, catalysis, sensor, and electrochemical energy storage.[178–180] In addition to the pseudocapacitance provided by metal groups in common MOFs, organic ligands in some MOFs can also undergo reversible redox reactions to provide pseudocapacitance. For example, Feng et al. synthesized a high-performance electrode based on two-dimensional metal-organic backbones (MOFs) derived from conductive hexaaminebenzene (HAB) through an electrophoretic deposition (EPD) process. The formation of HAB MOFs involved three consecutive steps: metal coordination with HAB ligands, base deprotonation of $-NH_2$ on HAB and oxidation of deprotonated HAB (Figure 18c). The authors chose Ni and Cu as metal ligands to synthesize two HAB MOFs. As is shown in Figure 18a, both MOFs showed distinct redox peaks in cyclic voltammograms, suggesting that the main charge storage mechanism comes from the pseudocapacitance of reversible redox reactions. Moreover, since both HAB MOFs show redox peaks similar to the organic ligands, the pseudocapacitance of the HAB MOFs was believed to mainly arising from their organic ligands. The presence of abundant amine groups in HAB (Figure 18b) allows MOFs to undergo the redox reactions. The sub-millimeter-thick pellets of Ni–HAB MOFs consequently showed a high bulk capacitance up to 760 $F cm^{-3}$ and a high

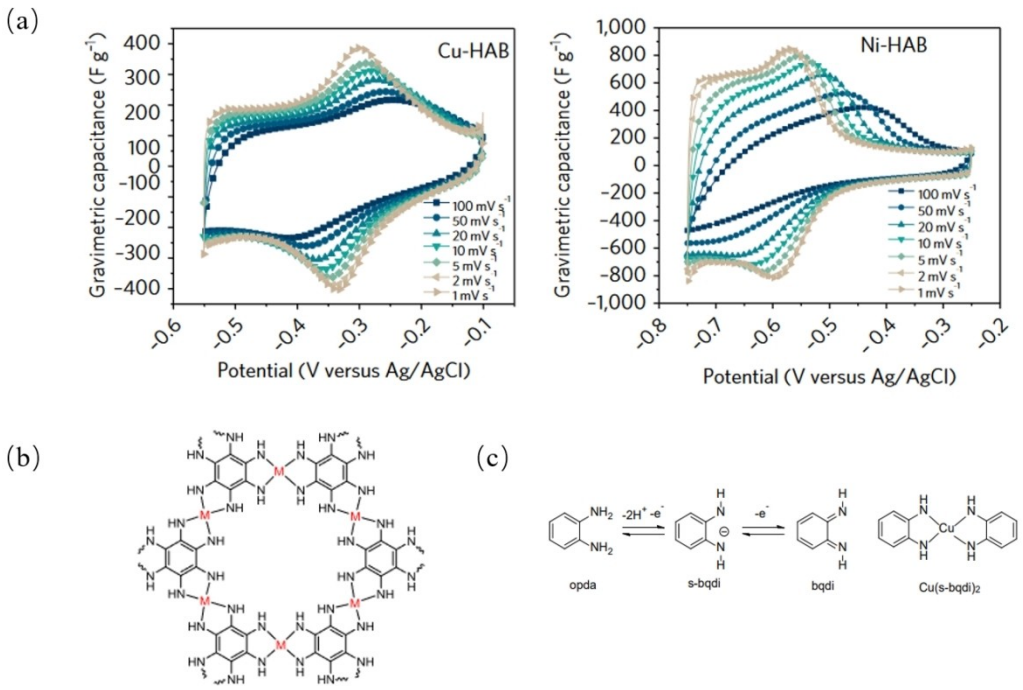

Figure 18. a) Cyclic voltammetry profiles collected at different scan rates for Cu–HAB and Ni–HAB electrodes. b) The structural of HAB MOF. c) The process of redox reaction of HAB MOF. Reproduced with permission from Ref. [181] Copyright (2018) The Author(s).

area capacitance over 20 F cm^{-2}, with the capacitance retention of 90% after 12,000 cycles.[181]

2.2.4. Others

There are also polymers that are not linear or framework-based, but used as electrode materials with redox-active sites for supercapacitors. Shi et al. used the organic precursors of hexaketocyclohexane octahydrate (HCO) and 3,3′-diaminobiphenylenediamine (DB) to produce a novel redox-active polymer (PDPZ) by a mild and facile dehydration Schiff base condensation. The obtained polymer was based on the structural unit of diquinoxaline-phenolic aldehyde. The broad redox peaks appeared in the CV plots (Figure 19a) indicated the pseudocapacitive active sites from PDPZ. A significant increase in the peak intensity of the C=N bond and a gradual decrease in the peak intensities of the C–N and N–H bond during the charging process were observed from the in situ Raman spectra. The same trend was also exhibited from the in situ IR spectra, indicating the energy storage sites arising from C=N groups. Besides, the molecular electrostatic potential (MESP) method revealed that the region near the imine part of the entire main chain structure of PDPZ exhibited a negative MESP value (Figure 19h), further implying that the C=N bonds were readily attracted to protons during the electrochemical process. Moreover, Figure 19i shows that the Gibbs free energy of the PDPZ molecule bound to the proton is much lower than ΔG for monovalent or multivalent metal ions in aqueous electrolytes, indicating that PDPZ possesses the strongest coordination ability with protons as charge carriers. All these results help infer that PDPZ is redox-active with excellent proton coordination ability which experiences highly reversible redox reactions between C=N and C–N/N–H bonds during the proton insertion/extraction process. The flexible supercapacitor assembled with PDPZ@MXene as the negative electrode and CuFePBA@MXene as the positive electrode achieved an excellent energy density of 64.3 mWh cm^{-3}, a power density of 6000 mW cm^{-3}, and a capacity retention rate of 98.2% after 10 000 cycles.[182]

2.3. Sulfur-containing groups

As compared to oxygen or nitrogen-containing functional groups, sulfur-containing groups are relatively less studied as redox-active groups in supercapacitors. Small molecules and framework-structured polymers that contain S-based functional groups to provide redox-active pseudocapacitance in supercapacitors were not found. Therefore, in this section, we only summarize S-containing functional groups in linear structured polymers and non-framework structured porous polymers for supercapacitors.

2.3.1. Linear-structured polymers

The most common linear polymers containing sulfur functional groups are polythiophene and its derivatives. PTh can be bipolar doped, but the n-doping process is more difficult compared to p-doping since it usually requires potentials as low as −2.0 V vs. Ag/Ag$^+$.[183] Nevertheless, PTh and its derivatives are promising electrode materials for supercapacitors and have attracted much attention due to their high electrical conductivity, high environmental stability, and long wavelength absorption.[9] The most studied thiophene-like molecules in supercapacitor are PTh and poly(3,4-ethylenedioxythiophene) (PEDOT), whose energy storage mechanisms are shown in Figure 20. Thiophene is a five-membered heterocyclic compound with a relatively high density of electron clouds on its ring, so it can be easily oxidized. Especially, under acidic conditions, the oxidation reaction is more likely to occur because H combines with the lone pair of electrons on sulfur, which destroys the aromatic structure and gives the ring the nature of a cyclic alkene.

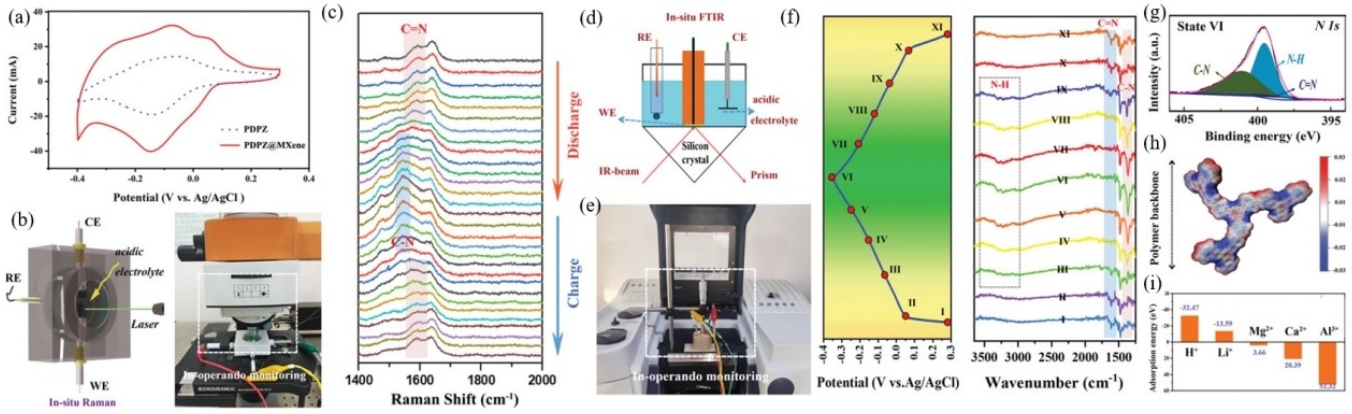

Figure 19. a) CV curves of the PDPZ and PDPZ@MXene electrodes tested in 2 M H_2SO_4 aqueous solution at 20 mV s^{-1}. b) In situ Raman test setup. c) In-situ Raman curves of PDPZ@MXene electrode. d) Schematic diagram of the in situ IR device. e) Photographs of the in situ IR device; f) GCD mapping and in situ FTIR mapping of the PDPZ@MXene electrode during discharge and charging. g) XPS mapping of N 1s in the fully discharged state. h) MESP distribution of the polymer backbone of the PDPZ. i) The adsorption energy of different charge carriers coordinated to the PDPZ molecule. Reproduced with permission from Ref. [182] Copyright (2022) Wiley-VCH GmbH.

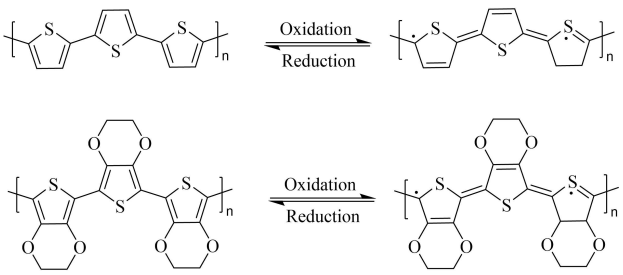

Figure 20. Energy storage mechanism of a) PTh, b) PEDOT.

In 1994, Laforgue et al. first applied conducting polymers to supercapacitor systems and found that poly-3-(4-fluorophenyl)-thiophene can be reversibly n-doped or p-doped and achieved a high charge density in 1 M of tetramethylammonium trifluoromethanesulfonate-acetonitrile solution.[184] In 2001, A. Laforgue et al. designed a hybrid supercapacitor using the conducting polymer poly(4-fluoropropyl-3-thiophene) as the positive electrode and activated carbon as the negative electrode. This supercapacitor was able to reach a maximum energy of 7.5 Wh kg^{-1} and to cycle 8000 times at 3.3 Wh kg^{-1}.[185]

Similar to PANI and PPy, the capacitive properties of PTh and its derivatives are morphological structure-dependent. Li et al. synthesized oriented poly(3,4-ethylenedioxythiophene) (PEDOT) micro/nanorod arrays through an electrochemical constant current method. The specific capacitances of PEDOT micro/nanorods, particles, and stacked blocks were observed to be 109.11, 72.52, and 36.77 F g^{-1} at 1 A g^{-1}, respectively.[186] Niu et al. prepared coral-like PEDOT nanotube arrays on carbon fibers using an electrochemical deposition technique. The electrode provided a specific capacitance of 184 F g^{-1} in 1 M H_2SO_4 electrolyte and maintaining 88% capacitance after 10000 cycles.[187] Chen et al. investigated the effects of various oxidants ($FeCl_3$, $Fe(Tos)_3$, and $MoCl_5$) on the molecular chain structure and capacitive properties of PEDOT prepared through a gas-phase polymerization process. They discovered that $Fe(Tos)_3$ can significantly increase the degree of oxidation and conjugate chain length of PEDOT, which increases the electrical conductivity and provides more active sites for the Faraday reaction. As a result, the PEDOT/P($Fe(Tos)_3$) electrode exhibited considerable conductivity (73 S cm^{-1}), high area capacitance (419 mF cm^{-2}) under different bending states, and achieved a good cycling stability (area capacitance of 60% of the initial value after 5000 cycles at 5 mA cm^{-2}).[188]

Doping of appropriate molecules/ions was also regarded as efficient pathway to enhance the electrochemical properties of PTh. Using a cationic surfactant-assisted dilute polymerization method, organic acid-doped conducting polymer nanomaterials, namely PTh–TA, were prepared by Subramania group. The assembled supercapacitor with the PTh–TA electrode showed a specific capacitance of 156 F g^{-1} at 1 mA cm^{-2}, an energy density of 14 Wh kg^{-1} at a power density of 522 W kg^{-1} and the capacity retention remained approximately 97% after 1000 cycles.[189] The doping of the organic acid yields nanostructured polymers with high specific surface area, which in turn leaded to the high capacitance. Wu et al. prepared a flexible Fe^{3+}-doped PTh electrode on carbon cloth through electrochemical deposition. The specific capacitance of the original PTh was 77.2 F g^{-1} at 0.5 A g^{-1}, while the Fe^{3+}-doping increased the specific capacitance to 108.1 F g^{-1} and the retention rate to 21.2% after 1000 charge/discharge cycles.[190]

Note that the thiophene-based polymers are also promising materials for other electrochemical applications in addition to supercapacitors. For example, Abigail et al reported a series of dioxythiophene-based polymers and investigated their redox application including pseudocapacitive and electrochromic behaviors.[191] Through tuning the backbone structure of these polymers using different thiophene-based comonomers, their redox properties can be finely manipulated. Strong electrochromic contrast with rapid optical switching times as well as high supercapacitor performance exhibiting charge/discharge behaviors with 70% retention of initial device capacitance after 15,000 charge/discharge cycles were achieved. Note that many redox molecules have the characteristics of redox transformations in electrochromic and supercapacitor devices, including polyaniline, polythiophene and their derivatives,[192] some microporous polymers such as triphenylamine (TPA)-derived polymers[193] and metallo-supramolecular polymers.[194]

Although the electrochemical properties of PTh and its derivatives can be optimized by morphology and structure adjustment, they still cannot behave as well as PANI or PPy due to their rapid decay of power density and specific capacitance. To overcome these drawbacks,[195] PThs have to combine with partners such as carbon materials or other electrochemically active components to reach a better performance when used in supercapacitors (Table 7).[15]

2.3.2. Porous organic polymers (POPs)

2.3.2.1. Non-framework structured POPs

Similar to nitrogen and oxygen, sulfur-containing functional groups can also provide pseudocapacitance through faradic reactions due to the fact that the lone pair of electrons on sulfur can combine with the cations in the electrolyte for redox reactions. Mohamed et al. constructed three porous organic polymers (POPs) without or with acetylene as the bridge – Bz–Th, TPA–Th, and P–Th–POPs (Figure 21a) by efficient coupling reactions with 1,3,5-tris(4,4,5,5-tetramethyl-1,3,2-dioxaborolan-2-yl) benzene (Bz-3BO), tris(4-(4,4,5,5-tetramethyl-1,3,2-dioxaborolan-2-yl)phenyl)amine (TPA-3BO), or 1,3,6,8-tetraethynylpyrene (P–T) using 2,8-dibromothiophene (Th–Br_2) as the building block. Due to the S heteroatoms and the unique morphological structure of the compound, the acetylene group containing P–Th–POP as a bridge showed a specific capacitance of 217 F g^{-1} at 0.5 A g^{-1} and an excellent cycling stability of more than 5000 cycles at 10 A g^{-1}.[161] Li et al. synthesized two porous organic polymers (POP-1 and POP-2) (Figure 21b) via the condensation synthesis of tetra(4-aminophenyl) methane and 2-thiophenecarboxaldehyde or 2,2-dithiophene-5-carboxaldehyde, both of which can undergo reversible redox reactions due to the presence of thiophene groups. It is shown that POP-

Table 7. Electrode materials based on PTh and PEDOT.

Materials	Preparation method	Electrolytes	Specific capacitance, current density	Capacity retention, Cycle number	Energy density [Wh kg^{-1}], power density [W kg^{-1}] (two-electrode)	Electrode system	Ref.
PTh/MWCNT	electropolymerization	0.5 M H_2SO_4	110 F g^{-1} at 1 A g^{-1}	90% (1000)	/	three	[196]
PTh-TNTs	electropolymerization	1 M H_2SO_4	640 F g^{-1} at 2 A g^{-1}	89% (1100)	237, 2100	three	[197]
PTh-g-rGO	esterification, oxidative polymerization	1 M H_2SO_4	230 F g^{-1} at 1 mV s^{-1}	100% (5000)	/	three	[198]
Fe^{3+}/PTh	electrochemical deposition	1 M H_2SO_4	108.1 F g^{-1} at 0.5 A g^{-1}	21.2% (1000)	/	three	[190]
GNPLs/PTh	*in situ* chemical polymerization	1 M H_2SO_4	960.71 F g^{-1} at 10 mV s^{-1}	84.9% (1500)	2.25, 23.55	three	[199]
PEDOT/NCC	electropolymerization	1 M KCl	117.02 F g^{-1} at 100 mV s^{-1}	86% (1000)	11.44, 99.85	three	[200]
PEDOT-NQS/MWCNT	enzymatic polymerization	1 M H_2SO_4	575 F g^{-1} at 5 mV s^{-1}	95% (1000)	/	three	[201]
TC@PEDOT	electrochemical deposition technology	1 M H_2SO_4	184 F g^{-1} at 100 mV s^{-1}	88% (10000)	/	three	[187]
PEDOT/P-($Fe(Tos)_3$)	gas phase polymerization	1 M H_2SO_4	413 mF cm^{-2} at 1 mA cm^{-2}	60% (5000)	/	three	[188]
PEDOT	electrodeposition process	PVA-LiCl	69.3 mF cm^{-2} at 0.1 mA cm^{-2}	97.8% (10000)	6.16 μWh cm^{-2}	two	[202]
PTh-TA	cationic surfactant assisted diluted polymerization	1 M $LiPF_6$	156 F g^{-1} at 1 mA cm^{-2}	97% (1000)	14, 522	two	[189]
PTh	surfactant assisted dilution	6 M KOH	273 F g^{-1} at 1 A g^{-1}	93% (2000)	54.6, 1700	two	[203]
PEDOT:PSS	drip method	sweat	8.94 F g^{-1} at 1 mV s^{-1}	75% (4000)	1.36, 329.70	two	[204]
PEDOT NFs@FKM	the soft template method	1 M Et_4NBF_4AN	776 mF cm^{-2} at 0.5 mA cm^{-2}	90.2% (10000)	11.8 mWh cm^{-3}, 0.0693 W cm^{-3}	two	[205]
e-PTh/Ti	electropolymerization	PVA-H_2SO_4	1357.31 mF g^{-1} at 5 mV s^{-1}	97% (3000)	23.11 mWh cm^{-2}, 90.44 mW cm^{-2}	two	[206]

2 has a well-formed, pore-rich rhombic topology and a higher BET specific surface area than POP-1. Therefore, it exhibited higher specific capacitance (332 F g^{-1}) and better cycling stability (over 90% capacity retention) as an electrode material for supercapacitors.[17]

2.4. Multiple redox-active groups

2.4.1. Small molecules

In addition to the ones with single species of redox-active groups, molecules with multiple functional groups can principally possess more potential for charge storage. Won et al. synthesized a quinone-containing conductive molecule 2,5-bis((2-(1H-indol-3-yl) ethyl) amine) cyclohexa-2,5-diene-1,4-dione (HBU) and fabricated a composite electrode by compounding it with activated carbon. As shown in Figure 22, the energy storage activity is derived from the redox-induced structural transition of the quinone and –NH groups (similar to the reversible redox process of nitrogen in a five-membered ring such as the pyrrole structure). The electrochemical specific capacitance of the supercapacitor with the composite electrode was then increased by ~130 F g^{-1} compared with the activated carbon-based electrode at 100 mV s^{-1} for 1000 cycles.[207]

2.4.2. Liner-structure polymers

In 1987, researchers synthesized poly(1,5-diamineanthraquinone) (PDAAQ), a bipolar doped molecule,[208] through electrochemical polymerization of 1,5-diamineanthraquinone. Due to the fully reversible redox pair (Figure 23) of 1,4-benzoquinone contained in the DAAQ molecule, PDAAQ exhibited robust electroactivity and high specific capacitance via fast reversible redox reactions in a wide potential window.[209]

PDAAQ can be further compounded with other materials and used as electrode materials for supercapacitor. Sun et al. synthesized graphene nanosheet/acid-treated multi-walled carbon nanotube-loaded poly(1,5-diamineanthraquinone) (GNS/aMWCNT@PDAAQ) composites using cerium sulfate ($Ce(SO_4)_2$) as the oxidizing agent and camphorsulfonic acid as the dopant.

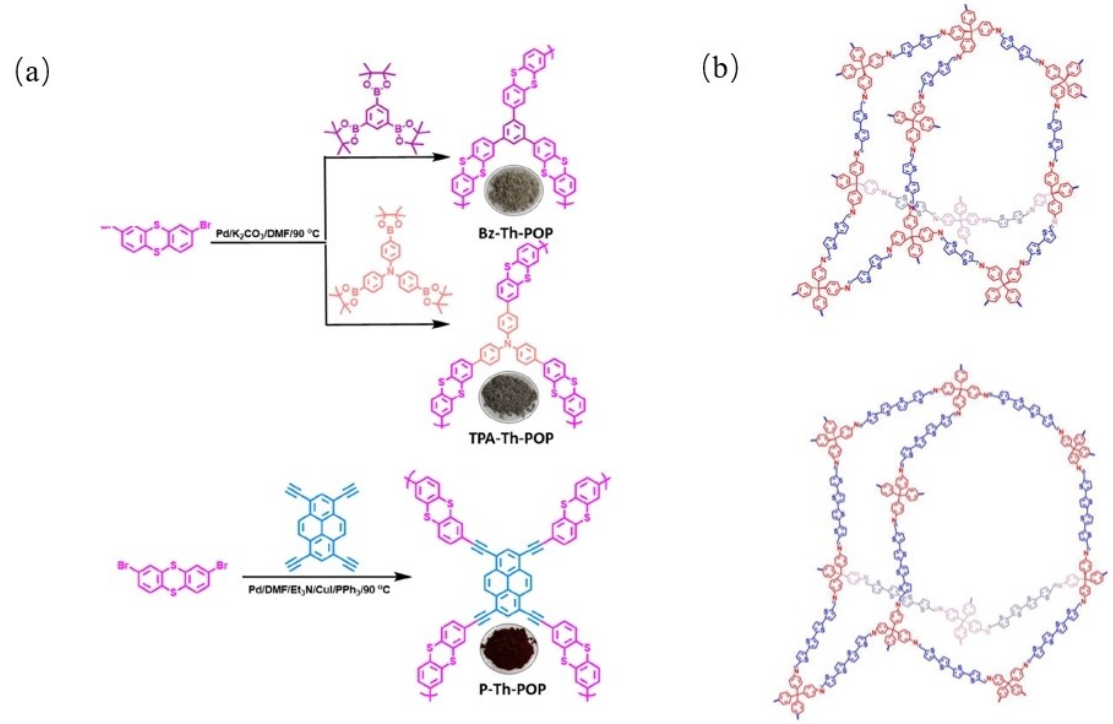

Figure 21. Synthesis route of a) Bz-3BO, TPA-3BO, Th–Br_2. Adapted with permission from Ref. [161] Copyright (2022) American Chemical Society. b) The structure of POP-1, POP-2. Adapted with permission from Ref. [17] Copyright (2018) Royal Society of Chemistry.

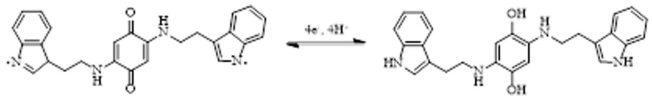

Figure 22. Mechanism for the charging and discharging of 2,5-bis((2-(1H-indol-3-yl) ethyl) amine) cyclohexa-2,5-diene-1,4-dione (HBU).[207]

The nanocomposites exhibited unique nanoporous morphology with high degree of π-conjugation and excellent conductive interpenetration network. It exhibited excellent cycling stability (only 7% of decay after 10,000 cycles) owing to its composition with carbon materials. In addition, due to the n-doping feature and the presence of abundant O-containing functional groups of PDAAQ, the supercapacitor assembled with GNS/aMWCNT@PDAAQ electrodes displayed excellent performances (an energy density of 55.5 Wh kg^{-1} at a power density of 153.9 kW kg^{-1}).[208] Besides, PDAAQ can also be applied to form flexible electrodes. Yang et al. reported a flexible supercapacitor consisting of a cross-linked polyvinylidene fluoride-hexafluoropropylene (PVDF-HFP) porous organic gel electrolyte and a carbon nanotube paper@poly(1,5-diamineanthraquinone) (CNT@PDAAQ) film electrode. Due to the p- and n-doping properties (Figure 24), the CNT@PDAAQ electrode exhibits good pseudocapacitive performance over a wide potential window. Specifically, as shown in the Figure 24, PAAQ is n-doped at the negative electrode and p-doped at the positive electrode and the prepared flexible SC device achieves an excellent bulk capacitance of 5.2 F cm^{-3} and a high energy density of 5.16 mWh cm^{-3} (41.4 Wh kg^{-1}).[210]

2.4.3. Porous organic polymers (POPs)

2.4.3.1. Framework structured POPs-COFs

Similarly, different variety of redox-active groups in COF can be simultaneously used as active sites for supercapacitors. Yang et al. developed a new arylamine linkage for the construction of COFs. Two new arylamine-linked COFs (AAm-TPB and AAm–Py) were prepared by condensation of cost-effective dimethyl succinate (DMSS) with the corresponding amines (TPB–NH_2 and Py–NH_2). The pseudocapacitive mechanism of AAm-TPB corresponds to the transition from benzoic acid diamine to quinone diimine and from enol to ketone (Figure 25). So, the AAm-TPB

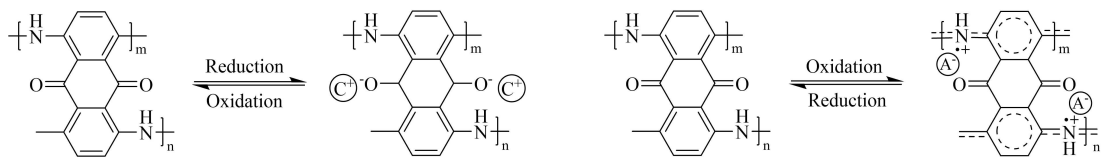

Figure 23. Mechanism of redox reaction of PDAAQ.[208]

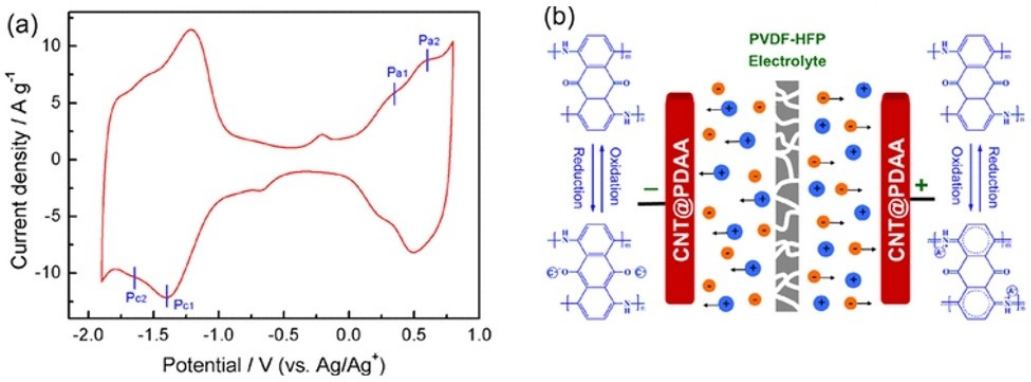

Figure 24. a) CV curve of the CNT@PDAAQ film electrode. b) Charge – discharge schematic illustration attaching corresponding redox reactions of CNT@PDAAQ film electrodes. Reproduced from Ref. [210] with permission. Copyright (2015) American Chemical Society.

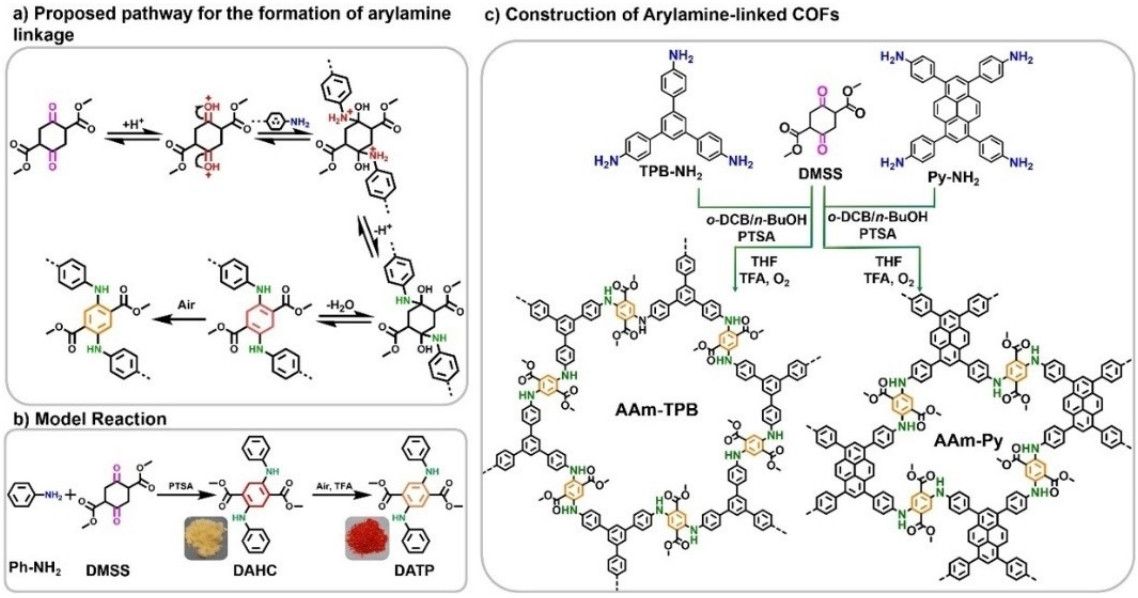

Figure 25. Reaction mechanism and synthetic of model compound DATP and arylamine-linked COFs. Reproduced from Ref. [211] with permission. Copyright (2021) Wiley-VCH GmbH.

electrode finally obtained a high capacitance of 271 F g^{-1} at 1 A g^{-1}.[211] El-Mahdy et al. constructed a hollow microtubular COF with a spongy structure using triazine and benzodiazole as the backbone through a template-free [3 + 2] condensation reaction of planar molecules 2,4,6-tris(4-formylphenyl) triazine (TPT-3CHO) and 2,5-diaminehydroquinone dihydrochloride (DAHQ-2HCl). Due to the presence of N and O atoms in the backbones that provide pseudocapacitance, a high specific capacitance of 256 F g^{-1} at 0.5 A g^{-1}, a capacitance retention of 98.8% after 1850 cycles, and a high energy density of 43 Wh kg^{-1} were obtained.[212]

2.4.3.2. Non-framework structured POPs

Similar to COFs, porous organic polymers that are not framework-structured can also introduce a variety of heteroatomic functional groups to improve the performance of supercapacitors. Weng et al. constructed NDTT, a single bond directly connected COF-like conjugated microporous polymer, by Stille coupling thiophene-substituted naphthalenediimide and triazine monomers (Figure 26). Due to the presence of triazine groups, imide groups and sulfur heteroatoms, the porous polymer electrode material achieved a capacitance of 425.3 F g^{-1} and an energy density of 33.2 Wh kg^{-1} at 0.2 A g^{-1}. The NDTT-based supercapacitor retained about 80.2% of the initial specific capacitance after 2000 cycles at a current density of 2 A g^{-1}.[213]

2.5. Others

In addition to the above-mentioned N/O/S-containing functional groups, some special structures of polymers applied to supercapacitors can also undergo redox reactions to provide pseudocapacitance. For example, due to the coplanar molecular

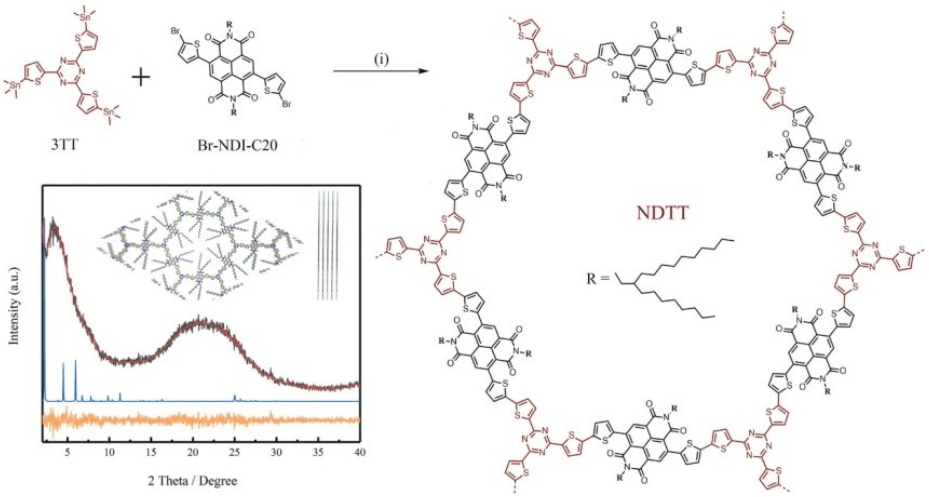

Figure 26. Synthesis route of NDTT. Reproduced from Ref. [213] with permission. Copyright (2022) Royal Society of Chemistry.

structure of the pyrene unit and the extended π-conjugated backbone, pyrene and its derivatives can achieve good stability and highly reversible doping/de-doping ability through a redox process as shown in Figure 27a. Bachman et al. compounded a derivative of pyrene with few-walled carbon nanotubes to form a nanostructured organic electrode. The surface redox reactions contributed to high pseudocapacitive performances of this pyrene-based electrode which finally exhibited an excellent energy density of 350 Wh kg^{-1} at a power density of 10 kW kg^{-1} for more than 10,000 cycles.[214] In addition to pyrene and its derivatives, azulene-based molecules can also act as pseudocapacitive electrode. Azulene is an aromatic hydrocarbon molecule composed of an electron-poor seven-membered ring and an electron-rich five-membered ring which form a fusion structure. The fusion structure between the two rings can produce an unusually large dipole moment in the molecule, giving good electrical conductivity and high charging capacity for the polymerized azulene, i.e., polyazulene (PAz) through redox-active doping mechanism as shown in Figure 27b.[215] For instance, Huang et al. synthesized a novel heterostructure PAz@$LaNiO_3$ based on chalcogenide oxide ($LaNiO_3$) nanosheets and poly(azulene). The as-prepared symmetric supercapacitor with PAz@$LaNiO_3$ electrodes exhibited a specific capacitance of up to 464 F g^{-1} at 2 A g^{-1} and provided an energy density of up to 56.4 Wh kg^{-1} at a power density of 1100 W kg^{-1}. Both $LaNiO_3$ and PAz were believed to contribute pseudocapacitance to the assembled supercapacitors.[216]

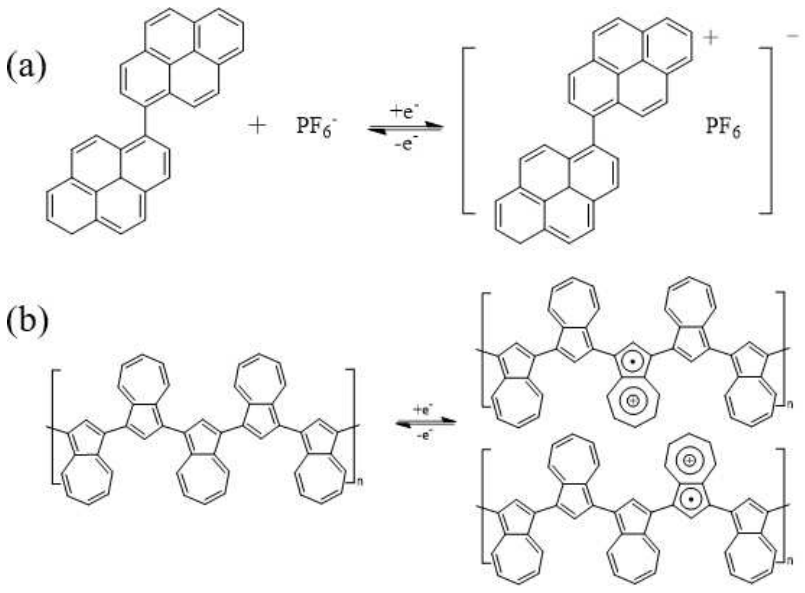

Figure 27. Redox - active mechanism of a) polypyrene, b) PAz.

3. Conclusions and Perspectives

Redox-active organics possess greater potential compared to inorganic electrode materials for high performance supercapacitors due to their abundant varieties, structural adjustability and good processability. Additionally, the use of organic materials also makes it possible to fabricate flexible supercapacitor devices. Redox-active organic molecules with low molecular weight generally suffer from low conductivity and high solubility in electrolytes which lead to low capacitance and cycling performance when used as pseudocapacitive materials. Composition with high conductive materials such as carbon is then usually adopted. In comparison to small molecules, the extended molecular structure of redox-active polymers allows them to be able to achieve higher conductivity and better cyclability.

In this review, we systematically summarize the organic materials with redox-active units that provide pseudocapacitance to supercapacitors. Redox-active molecules with short molecular chain, i.e., small molecules or extended molecular structure, i.e., polymers that are adopted as electrode materials have been summarized. The latter is further classified into linear polymers and polymers with non-linear extended structures, mainly including POPs that are framework-structured (e.g., COFs, MOFs), and non-framework-structured, and others. Furthermore, we present the classification and preparation of these organic molecules with redox-active properties arising from N, O or/and S-containing groups, and focus on the relationship between their pseudocapacitive behaviors and how these redox-active functional groups contribute to the energy storage process.

Note that both pseudocapacitive and battery-type materials store energy by means of redox reactions. The reactions of battery-type materials occur in bulk-phase which are diffusion-controlled and usually slow during electrochemical processes. In contrast, the reactions of pseudocapacitive materials taking places at the surfaces of electrode are generally fast processes. Pseudocapacitive materials can be further categorized into intrinsic and non-intrinsic. The intrinsic pseudocapacitive materials store charges by fast redox reactions or fast embedding/de-embedding of ions occurring at/near the electrode surfaces. While the non-intrinsic pseudocapacitive materials are obtained from the conventional battery-type materials through nanoengineering treatment and exhibit pseudocapacitive properties only at the nanoscale. Indeed, electrode materials with nanoscale sizes are able to expose more surfaces for the electrochemical reactions than the bulk materials. Therefore, the battery-type materials which usually experience slow bulk reactions will exhibit pseudocapacitive features when their sizes decrease to nanoscale.

The energy storage mechanism based on surficial redox reactions makes the pseudocapacitive materials achieve high capacitance and excellent rate performance since the ion storage process is not restricted by processes such as diffusion, phase transition, etc. Meanwhile, from the experimental point of view, pseudocapacitive materials exhibit characteristics which can be distinguished from battery-type materials using analytical test methods such as cyclic voltammetry, constant current charge/discharge test, and reaction kinetic analysis[217] (Figure 28). Specifically, from the CV curves, the battery-type material shows fine sharp peaks, while the surface redox pseudocapacitance exhibits a quasi-rectangular shape similar to that of the capacitive material, and the intercalation pseudocapacitance shows symmetrical broad peaks superimposed on the rectangular contour and the anodic and cathodic peaks are almost at the same potential, which is different from that of the battery-type material. Furthermore, the charging and discharging platforms of the GCD curves show consistent results as

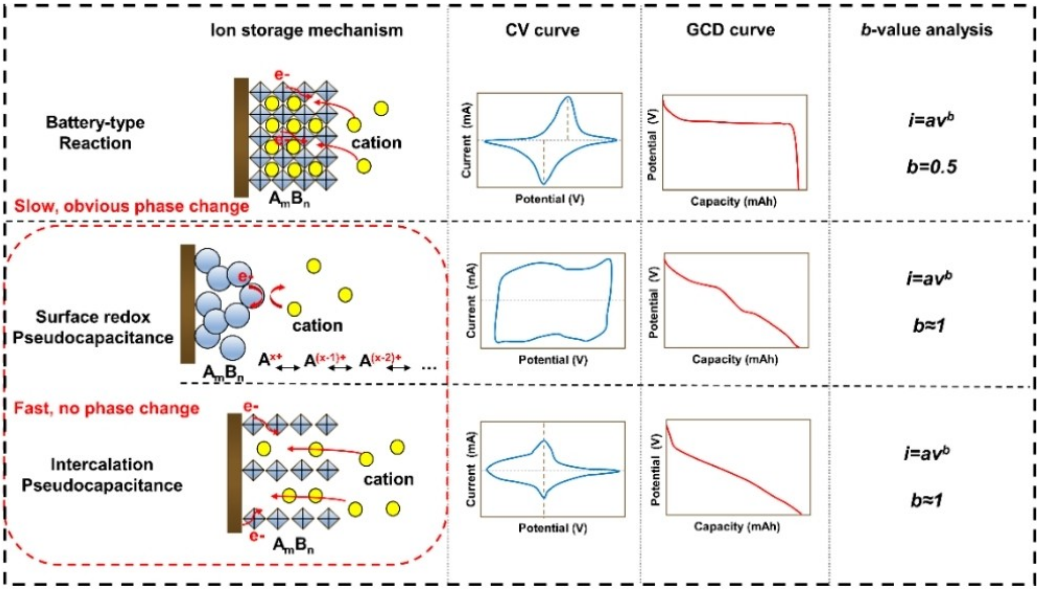

Figure 28. Energy storage mechanism and characteristics of battery-type materials and pseudocapacitive materials. Reproduced with permission from Ref. [217]. Copyright (2022) American Chemical Society.

those of the CV curves. Based on CV profiles, the kinetic analysis can be expressed by the quantitative relationship between the current response and the corresponding sweep rate: $i(v) = av^b$,[218] where v is the sweep rate, $i(v)$ is the current response, a is a constant and b is a parameter related to the charge storage mechanism. Specifically, the b value approaching 0.5 indicates the electrode reaction a diffusion-controlled battery-type response, while when b value equals to 1, it indicates a surface controlled capacitive process.[219]

Though many efforts have been paid, to design redox-active materials with high pseudocapacitance and fabricate supercapacitor devices with energy densities that are comparable to LIBs are still far on the way and need more endeavors:

1) Abundant redox-active groups present in the materials involving multiple-electron reactions can in principle increase the capacitance of the electrode but an efficient utilization of them needed to be concerned. Organic macromolecules with rich pore structure, for example POPs, to highly expose the active groups is demanded. Among varieties of POPs, the ones with regular framework structure such as COFs and MOFs, can further facilitate the transport and storage of ions due to their ordered pore structure that can form long-range channels for charge transportation. In addition, the modulation of the morphology is also a way to expose the active sites in organic materials. Nanostructure engineering and the avoidance of stacking are often adopted strategies to access more active sites. At the same time, by regulating the surface wettability through group functionalization, the electrode materials can be further designed to be affinitive to the electrolytes and promote the electrochemical process.
2) In addition to massive accessible active sites, electronic conductivity of the organic materials is also a key factor need to be considered since electrochemical redox reactions involve the participation of electrons on the active units. To combine organic electrode materials with highly conductive agents, most commonly carbons, is proved to be very helpful but this extra introduction of component with relatively low capacitance is not desirable. Therefore, to synthesize pseudocapacitive materials with intrinsic electron conductivity from the molecular or atomic level is expected. Specifically, the design of conjugated structures plays a great role on the enhancement of their conductivity due to the extended delocalized space for electrons. In this case, small molecules take no advantages owing to their short molecular chain not to mention that they are extremely soluble in the electrolytes, resulting in poor cycling stability. Therefore, conjugated macromolecules with extended structure that can achieve relatively higher conductivity and better capacitance retention are desirable as electrode materials. Nevertheless, to synthesize organic electrode materials with high energy storage capability, excellent electronic conductivity and long-period structural stability still needs a better understanding of the design principles, i.e., the relationship between their structures and the electrochemical performances from microstructure to macroscopic level.
3) In this case, theoretical calculations represent one kind of essential method to provide a guidance for molecular design. Through computational calculations, researchers can, for example, simulate the electronic structure of a material, explain conductivity and kinetic differences between materials, calculate adsorption/binding energy and ion diffusion properties, and other factors related to the energy storage mechanism. It provides a support for experimental results, unravels important atomic-scale characteristics towards material properties, and thus allows researchers gain more molecular insights into preferred structures of the electrode materials for supercapacitors. In addition to theoretical simulation, a more direct detection and unveiling of structure-property relationship of the redox-active electrode materials based on experimental methods is also highly demanded. In situ or operando characterization is regarded as an effective technology but currently still not widely used to gain the detailed pseudocapacitive expression of electrode.
4) The molecular design of an effective electrode materials is the very first step towards high performance supercapacitors for application. Cost effectiveness of the synthetic process and adaptability for industrial production are also indispensable towards a large-scale application of supercapacitors. Currently, most organic polymer materials (especially framework polymers such as COFs) are synthesized under harsh conditions with high cost. It is therefore crucial to develop facile synthetic procedures requiring low energy consumption and adopt monomer precursors that are rich in sources with low price. Moreover, from the device point of view, compatible electrolytes that can effectively reduce the solubility of the organic electrode materials but improve the ionic conductivity during charging/discharging process is also important. While a broadened voltage window that matches the electrodes and electrolytes are critical to fabricate supercapacitors with high energy densities.
5) Last but not the least, as the application scenarios become diverse and complicated, supercapacitor devices are also designed to be smarter with multi-functionality. Flexible and stretchable supercapacitors, for example, are highly demanded in the application of wearable electronic devices. To go a step further, supercapacitors with self-healing functions that resist to physical or/and chemical damage make them more sophisticated and durable during long-term service period. In this case, organic electrode materials are granted to be suitable without a doubt due to their softer mechanical properties, high safety and chemical diversity with more possibility to be designed from the atomic and molecular level as compared to the inorganics. However, due to the low tap densities of organic materials, low areal mass loading is usually adopted to test the performance of organic electrodes in laboratory. This will lead to a low volumetric energy density of the organic materials which is what we do not want to see for practical purposes. Indeed, volumetric energy density is an important parameter for practical application especially when the energy storage devices are used in portable or miniature

electronic scenarios. Therefore, to increase the tap density of the organic electrodes to achieve an improved volumetric enegy density is of great importance and has practical significance. To increase the space utilization efficiency of the electrode, one can in principle adjust the parameters of the organic materials such as particle size, porosity, surface area and so on from the material-level, or optimize the processing conditions from the practical point of view. Nevertheless, the adjustment of these parameters may have a negative effect since they also affect the distribution of the binder and conductive materials and the diffusion of electrolyte ions in the electrodes which possibly result in inferior electrochemical properties of the organic electrodes. Based on the afore-mentioned aspects regarding organic electrodes and with the practical application in consideration, economic and functionalized efficiency for material synthesis and device production on the premise that their energy and power densities are not sacrificed is necessary and still has a long way to go.

Acknowledgements

The National Natural Science Foundation of China (52073170, 22279078), Shanghai Municipal Education Commission (Innovation Program (2019-01-07-00-09-E00021)) and Innovative Research Team of High-level Local Universities in Shanghai are acknowledged for the financial support.

Conflict of Interests

There are no conflicts to declare.

Keywords: energy storage systems · supercapacitor · redox-active groups · organic electrode materials · pseudocapacitance

[1] Poonam, K. Sharma, A. Arora, S. K. Tripathi, *J. Energy Storage* **2019**, *21*, 801–825.
[2] N. N. Loganathan, V. Perumal, B. R. Pandian, R. Atchudan, T. N. J. I. Edison, M. Ovinis, *J. Energy Storage* **2022**, *49*, 104149.
[3] S. Biswas, A. Chowdhury, *ChemPhysChem* **2023**, *24*, e202200567.
[4] S. Sharma, P. Chand, *Results Chem.* **2023**, *5*, 100885.
[5] S. P. Ega, P. Srinivasan, *J. Energy Storage* **2022**, *47*, 103700.
[6] S. Raj K A, C. S. Rout, *J. Mater. Chem. A* **2023**, *11*, 5495–5519.
[7] C. An, Y. Zhang, H. Guo, Y. Wang, *Nanoscale Adv.* **2019**, *1*, 4644–4658.
[8] T. B. Schon, B. T. McAllister, P.-F. Li, D. S. Seferos, *Chem. Soc. Rev.* **2016**, *45*, 6345–6404.
[9] Q. Meng, K. Cai, Y. Chen, L. Chen, *Nano Energy* **2017**, *36*, 268–285.
[10] S. Wustoni, D. Ohayon, A. Hermawan, A. Nuruddin, S. Inal, Y. S. Indartono, B. Yuliarto, *Polym. Rev.* **2023**, DOI: 10.1080/15583724.2023.2220131.
[11] A. Varghese, S. Devi K R, F. Kausar, D. Pinheiro, *Mater. Today Chem.* **2023**, *29*, 101424.
[12] I. Ul Hoque, R. Holze, *Polymer* **2023**, *15*, 730.
[13] X. Liu, C. Liu, W. Lai, W. Huang, *Adv. Mater. Technol.* **2020**, 2000154.
[14] R. Khan, Y. Nishina, *Nanoscale* **2021**, *13*, 36–50.
[15] X. Zhang, Z. Xiao, X. Liu, P. Mei, Y. Yang, *Renewable Sustainable Energy Rev.* **2021**, *147*, 111247.
[16] Q. Meng, K. Cai, Y. Chen, L. Chen, *Nano Energy* **2017**, *36*, 268–285.
[17] T. Li, W. Zhu, R. Shen, H.-Y. Wang, W. Chen, S.-J. Hao, Y. Li, Z.-G. Gu, Z. Li, *New J. Chem.* **2018**, *42*, 6247–6255.
[18] A. Mauger, C. Julien, A. Paolella, M. Armand, K. Zaghib, *Materials* **2019**, *12*, 1770.
[19] M. Wang, H. Guo, R. Xue, Q. Li, H. Liu, N. Wu, W. Yao, W. Yang, *ChemElectroChem* **2019**, *6*, 2984–2997.
[20] Q. Li, M. Horn, Y. Wang, J. MacLeod, N. Motta, J. Liu, *Materials* **2019**, *12*, 703.
[21] R. Holze, *Polymer* **2020**, *12*, 1835.
[22] S. Kumar, G. Saeed, L. Zhu, K. N. Hui, N. H. Kim, J. H. Lee, *Chem. Eng. J.* **2021**, *403*, 126352.
[23] Y. Lu, Y. Cai, Q. Zhang, J. Chen, *Adv. Mater.* **2022**, *34*, 2104150.
[24] L. Deng, C. Zhou, Z. Ma, G. Fan, *J. Colloid Interface Sci.* **2020**, *561*, 416–425.
[25] M. Boota, C. Chen, M. Bécuwe, L. Miao, Y. Gogotsi, *Energy Environ. Sci.* **2016**, *9*, 2586–2594.
[26] X. He, X. Zhang, *J. Energy Storage.* **2022**, *56*, 106023.
[27] S. Chaudhary, M. Raja, O. P. Sinha, *Adv. Nat. Sci. Nanosci. Nanotechnol.* **2021**, *12*, 015011.
[28] M. Li, R. P. Hicks, Z. Chen, C. Luo, J. Guo, C. Wang, Y. Xu, *Chem. Rev.* **2023**, *123*, 1712–1773.
[29] T. Brousse, C. Cougnon, D. Bélanger, *J. Braz. Chem. Soc.* **2018**, *29*, 989–997.
[30] K. W. Leitner, B. Gollas, M. Winter, J. O. Besenhard, *Electrochim. Acta* **2004**, *50*, 199–204.
[31] K. Kalinathan, D. P. DesRoches, X. Liu, P. G. Pickup, *J. Power Sources* **2008**, *181*, 182–185.
[32] B. Guo, Z. Hu, Y. An, N. An, P. Jia, Y. Zhang, Y. Yang, Z. Li, *RSC Adv.* **2016**, *6*, 40602–40614.
[33] S. Li, X. Wang, L. Hou, X. Zhang, Y. Zhou, Y. Yang, Z. Hu, *Electrochim. Acta* **2019**, *317*, 437–448.
[34] D. M. Anjos, J. K. McDonough, E. Perre, G. M. Brown, S. H. Overbury, Y. Gogotsi, V. Presser, *Nano Energy* **2013**, *2*, 702–712.
[35] L. Hou, Z. Hu, H. Wu, X. Wang, Y. Xie, S. Li, F. Ma, C. Zhu, *Dalton Trans.* **2019**, *48*, 9234–9242.
[36] G. Pognon, C. Cougnon, D. Mayilukila, D. Bélanger, *ACS Appl. Mater. Interfaces* **2012**, *4*, 3788–3796.
[37] J. Shi, Z. Zhao, J. Wu, Y. Yu, Z. Peng, B. Li, Y. Liu, H. Kang, Z. Liu, *ACS Sustainable Chem. Eng.* **2018**, *6*, 4729–4738.
[38] H. Zhang, L. Wang, X. Xing, S. Zhao, K. Wang, S. (Frank) Liu, *Adv. Funct. Mater.* **2022**, *32*, 2208403.
[39] J. Liu, Y. Yuan, H. Fang, Y. Xu, W. Sun, S. Chen, Y. Wang, L.-P. Lv, *ACS Appl. Energ. Mater.* **2022**, *5*, 8112–8122.
[40] W. Zhang, H. Liu, H. Kang, S. Zhang, B. Yang, Z. Li, *Electrochim. Acta* **2023**, *448*, 142194.
[41] Y. Yang, D. Qian, P. Liang, Z. Zhang, Z. Li, Z. Hu, *Diamond Relat. Mater.* **2022**, *125*, 108961.
[42] C. Zhou, T. Gao, Q. Liu, Y. Wang, D. Xiao, *Electrochim. Acta* **2020**, *336*, 135628.
[43] H. Itoi, Y. Yasue, K. Suda, S. Katoh, H. Hasegawa, S. Hayashi, M. Mitsuoka, H. Iwata, Y. Ohzawa, *ACS Sustainable Chem. Eng.* **2017**, *5*, 556–562.
[44] A. Mendez, S. Isikli, R. Diaz, *Electrochemistry* **2013**, *81*, 853.
[45] L. Hou, C. Kong, Z. Hu, Y. Han, B. Wu, *J. Electroanal. Chem.* **2021**, *895*, 115402.
[46] L. Xu, R. Shi, H. Li, C. Han, M. Wu, C.-P. Wong, F. Kang, B. Li, *Carbon* **2018**, *127*, 459–468.
[47] X. Yang, Y. Yang, Q. Zhang, X. Wang, Y. An, B. Guo, Z. Hu, H. Wu, *RSC Adv.* **2017**, *7*, 48341–48353.
[48] S. Isikli, R. Díaz, *J. Power Sources* **2012**, *206*, 53–58.
[49] R. Shi, C. Han, H. Duan, L. Xu, D. Zhou, H. Li, J. Li, F. Kang, B. Li, G. Wang, *Adv. Energy Mater.* **2018**, *8*, 1802088.
[50] M. Shi, C. Peng, X. Zhang, *Small* **2023**, *19*, 2301449.
[51] Y. Yang, W. Ma, H. Zhu, H. Meng, C. Wang, F. Ma, Z. Hu, *New J. Chem.* **2020**, *44*, 16821–16830.
[52] G. Ma, F. Hua, K. Sun, E. Feng, Z. Zhang, H. Peng, Z. Lei, *Ionics* **2018**, *24*, 549–561.
[53] S. P. Ega, M. R. Biradar, P. Srinivasan, S. V. Bhosale, *Electrochim. Acta* **2020**, *357*, 136835.
[54] Y. Yang, D. Qian, J. Yang, Y. Xiong, Z. Zhang, Z. Li, Z. Hu, *Chem. Eng. Sci.* **2023**, *265*, 118272.
[55] S. Li, Y. Zhou, Z. Hu, X. Meng, H. Shi, X. Zhang, G. Hou, J. Zhu, J. Wang, *ACS Appl. Energ. Mater.* **2023**, *6*, 4788–4799.
[56] S. D. Jagdale, C. R. K. Rao, S. V. Bhosale, S. V. Bhosale, *J. Energy Storage* **2023**, *66*, 107482.
[57] Y. Katsuyama, Y. Nakayasu, K. Oizumi, Y. Fujihara, H. Kobayashi, I. Honma, *Adv. Sustainable Syst.* **2019**, *3*, 1900083.

[58] B. Guo, Y. Yang, Z. Hu, Y. An, Q. Zhang, X. Yang, X. Wang, H. Wu, *Electrochim. Acta* **2017**, *223*, 74–84.
[59] N. An, Z. Hu, H. Wu, Y. Yang, Z. Lei, W. Dong, *J. Mater. Chem. A* **2017**, *5*, 25420–25430.
[60] Z. Chang, A. Huang, X. An, X. Qian, *Carbohydr. Polym.* **2020**, *244*, 116442.
[61] L. Gao, S. Gan, H. Li, D. Han, F. Li, Y. Bao, L. Niu, *Nanotechnology* **2017**, *28*, 275602.
[62] A. Rudge, J. Davey, I. Raistrick, S. Gottesfeld, J. P. Ferraris, *J. Power Sources* **1994**, *47*, 89–107.
[63] W. Lee, S. Suzuki, M. Miyayama, *Nanomaterials* **2014**, *4*, 599–611.
[64] S. Wang, Y. Guo, F. Wang, S. Zhou, T. Zeng, Y. Dong, *New. Carbon. Mater.* **2022**, *37*, 109–135.
[65] M. M. Samy, M. G. Mohamed, A. F. M. EL-Mahdy, T. H. Mansoure, K. C.-W. Wu, S.-W. Kuo, *ACS Appl. Mater. Interfaces* **2021**, *13*, 51906–51916.
[66] C. R. DeBlase, K. E. Silberstein, T.-T. Truong, H. D. Abruña, W. R. Dichtel, *J. Am. Chem. Soc.* **2013**, *135*, 16821–16824.
[67] S. Chandra, D. Roy Chowdhury, M. Addicoat, T. Heine, A. Paul, R. Banerjee, *Chem. Mater.* **2017**, *29*, 2074–2080.
[68] A. Khayum M, V. Vijayakumar, S. Karak, S. Kandambeth, M. Bhadra, K. Suresh, N. Acharambath, S. Kurungot, R. Banerjee, *ACS Appl. Mater. Interfaces* **2018**, *10*, 28139–28146.
[69] A. Halder, M. Ghosh, A. Khayum M, S. Bera, M. Addicoat, H. S. Sasmal, S. Karak, S. Kurungot, R. Banerjee, *J. Am. Chem. Soc.* **2018**, *140*, 10941–10945.
[70] M. Li, J. Liu, Y. Li, G. Xing, X. Yu, C. Peng, L. Chen, *CCS Chem.* **2021**, *3*, 696–706.
[71] T.-L. Yang, J.-Y. Chen, S.-W. Kuo, C.-T. Lo, A. F. M. El-Mahdy, *Polymer* **2022**, *14*, 3428.
[72] Q. Hao, Y. Tao, X. Ding, Y. Yang, J. Feng, R.-L. Wang, X.-M. Chen, G.-L. Chen, X. Li, H. OuYang, X. Hu, J. Tian, B.-H. Han, G. Zhu, W. Wang, F. Zhang, B. Tan, Z.-T. Li, D. Wang, L.-J. Wan, *Sci. China Chem.* **2023**, *66*, 620–682.
[73] Y. Zhang, S. N. Riduan, *Chem. Soc. Rev.* **2012**, *41*, 2083–2094.
[74] Y. Liao, H. Wang, M. Zhu, A. Thomas, *Adv. Mater.* **2018**, *30*, 1705710.
[75] V. C. Wakchaure, A. R. Kottaichamy, A. D. Nidhankar, K. C. Ranjeesh, M. A. Nazrulla, M. O. Thotiyl, S. S. Babu, *ACS Appl. Energ. Mater.* **2020**, *3*, 6352–6359.
[76] N. An, Z. Guo, C. Guo, M. Wei, D. Sun, Y. He, W. Li, L. Zhou, Z. Hu, X. Dong, *Chem. Eng. J.* **2023**, *458*, 141434.
[77] X.-C. Li, Y. Zhang, C.-Y. Wang, Y. Wan, W.-Y. Lai, H. Pang, W. Huang, *Chem. Sci.* **2017**, *8*, 2959–2965.
[78] L. Li, F. Lu, H. Guo, W. Yang, *Microporous Mesoporous Mater.* **2021**, *312*, 110766.
[79] Y. Kou, Y. Xu, Z. Guo, D. Jiang, *Angew. Chem. Int. Ed.* **2011**, *50*, 8753–8757.
[80] G. S. D. Reis, H. P. D. Oliveira, S. H. Larsson, M. Thyrel, E. Claudio Lima, *Nanomaterials* **2021**, *11*, 424.
[81] Y. Deng, Y. Xie, K. Zou, X. Ji, *J. Mater. Chem. A* **2016**, *4*, 1144–1173.
[82] K. Qin, J. Huang, K. Holguin, C. Luo, *Energy Environ. Sci.* **2020**, *13*, 3950–3992.
[83] S. Eigler, A. Hirsch, *Angew. Chem. Int. Ed.* **2014**, *53*, 19.
[84] Y. Xu, X. Chen, C. Huang, Y. Zhou, B. Fan, Y. Li, A. Hu, Q. Tang, K. Huang, *J. Power Sources* **2021**, *488*, 229426.
[85] M. M. Sk, C. Y. Yue, *RSC Adv.* **2014**, *4*, 19908.
[86] X. Lu, L. Li, B. Song, K. Moon, N. Hu, G. Liao, T. Shi, C. Wong, *Nano Energy* **2015**, *17*, 160–170.
[87] Y. Zhao, X. Wang, N. Wang, M. Li, Q. Li, J. Liu, *J. Phys. Chem. C* **2019**, *123*, 994–1002.
[88] Y. Zhao, J. Liu, N. Wang, Q. Li, M. Hu, *J. Mater. Chem. A* **2018**, *6*, 7566–7572.
[89] W. Cui, Y. Zheng, R. Zhu, Q. Mu, X. Wang, Z. Wang, S. Liu, M. Li, R. Ran, *Adv. Funct. Mater.* **2022**, *32*, 2204823.
[90] H. Wang, H. Wu, Y. Chang, Y. Chen, Z. Hu, *Chin. Sci. Bull.* **2011**, *56*, 2092–2097.
[91] Y. He, X. Yang, N. An, X. Wang, Y. Yang, Z. Hu, *New J. Chem.* **2019**, *43*, 1688–1698.
[92] M. Khalid, A. Hassan, A. M. B. Honorato, F. N. Crespilho, H. Varela, *J. Electroanal. Chem.* **2019**, *847*, 113193.
[93] W. Zhang, Y. Li, H. Kang, B. Yang, Z. Li, H. Liu, *Electrochim. Acta* **2022**, *404*, 139725.
[94] F. Li, X. Wang, R. Sun, *J. Mater. Chem. A* **2017**, *5*, 20643–20650.
[95] M. Ates, E. Özten, *Plast. Rubber Compos.* **2018**, *47*, 192–201.
[96] M. Ates, S. Caliskan, E. Özten, *J. Solid State Electrochem.* **2018**, *22*, 3261–3271.
[97] H. Heli, H. Yadegari, *J. Electroanal. Chem.* **2014**, *713*, 103–111.
[98] H. Heli, H. Yadegari, A. Jabbari, *Mater. Chem. Phys.* **2012**, *134*, 21–25.
[99] A. Ehsani, M. G. Mahjani, M. Jafarian, *Synth. Met.* **2011**, *161*, 1760–1765.
[100] J. Li, Y. Sun, D. Li, H. Yang, X. Zhang, B. Lin, *J. Alloys Compd.* **2017**, *708*, 787–795.
[101] D. Li, Y. Liu, B. Lin, C. Lai, Y. Sun, H. Yang, X. Zhang, *RSC Adv.* **2015**, *5*, 98278–98287.
[102] Z. Liu, H. Zhou, Z. Huang, W. Wang, F. Zeng, Y. Kuang, *J. Mater. Chem. A* **2013**, *1*, 3454.
[103] P. Tamailarasan, S. Ramaprabhu, *J. Phys. Chem. C* **2012**, *116*, 14179–14187.
[104] J. Jaidev, S. Ramaprabhu, *J. Mater. Chem.* **2012**, *22*, 18775–18783.
[105] R. B. Choudhary, S. Ansari, M. Majumder, *Renewable Sustainable Energy Rev.* **2021**, *145*, 110854.
[106] R. B. Choudhary, S. Ansari, B. Purty, *J. Energy Storage* **2020**, *29*, 101302.
[107] A. Clemente, *Solid State Ionics* **1996**, *85*, 273–277.
[108] D. P. Dubal, N. R. Chodankar, Z. Caban-Huertas, F. Wolfart, M. Vidotti, R. Holze, C. D. Lokhande, P. Gomez-Romero, *J. Power Sources* **2016**, *308*, 158–165.
[109] J. Zhao, J. Wu, B. Li, W. Du, Q. Huang, M. Zheng, H. Xue, H. Pang, *Prog. Nat. Sci.* **2016**, *26*, 237–242.
[110] T. Wang, Y. Wang, D. Zhang, X. Hu, L. Zhang, C. Zhao, Y.-S. He, W. Zhang, N. Yang, Z.-F. Ma, *ACS Appl. Mater. Interfaces* **2021**, *13*, 17726–17735.
[111] Y. Wang, Y. Shi, L. Pan, Y. Ding, Y. Zhao, Y. Li, Y. Shi, G. Yu, *Nano Lett.* **2015**, *15*, 7736–7741.
[112] M. Zhang, Y. Song, D. Yang, Z. Qin, D. Guo, L. Bian, X. Sang, X. Sun, X. Liu, *Adv. Funct. Mater.* **2021**, *31*, 2006203.
[113] Q. Ding, X. Xu, Y. Yue, C. Mei, C. Huang, S. Jiang, Q. Wu, J. Han, *ACS Appl. Mater. Interfaces* **2018**, *10*, 27987–28002.
[114] Z.-H. Chang, D.-Y. Feng, Z.-H. Huang, X.-X. Liu, *Chem. Eng. J.* **2018**, *337*, 552–559.
[115] S. Dhibar, A. Roy, S. Malik, *Eur. Polym. J.* **2019**, *120*, 109203.
[116] X. Zhang, J. Zhang, Y. Chen, K. Cheng, J. Yan, K. Zhu, K. Ye, G. Wang, L. Zhou, D. Cao, *J. Colloid Interface Sci.* **2019**, *536*, 291–299.
[117] P. Bhardwaj, S. Singh, P. R. Kharangarh, A. N. Grace, *Diamond Relat. Mater.* **2020**, *108*, 107989.
[118] S. Dhibar, S. Malik, *ACS Appl. Mater. Interfaces* **2020**, *12*, 54053–54067.
[119] L. Luo, X. Wang, S. Yang, J. Dai, D. Li, L. Xia, C. Chi, A. Cabot, Y. Xu, L. Dai, *ACS Appl. Energ. Mater.* **2023**, *6*, 5940–5951.
[120] C. Lv, X. Ma, R. Guo, D. Li, X. Hua, T. Jiang, H. Li, Y. Liu, *Energy* **2023**, *270*, 126830.
[121] R. Gonçalves, R. S. Paiva, T. M. Lima, M. W. Paixão, E. C. Pereira, *Electrochim. Acta* **2021**, *368*, 137570.
[122] S. K. Ponnaiah, P. Prakash, *Int. J. Hydrogen Energy* **2021**, *46*, 19323–19337.
[123] S. Alireza Hashemi, S. Mojtaba Mousavi, H. Reza Naderi, S. Bahrani, M. Arjmand, A. Hagfeldt, W.-H. Chiang, S. Ramakrishna, *Chem. Eng. J.* **2021**, *418*, 129396.
[124] Y. Wang, C. Xiang, Y. Zou, F. Xu, L. Sun, J. Zhang, *J. Energy Storage* **2021**, *41*, 102838.
[125] J. Ren, M. Shen, Z. Li, C. Yang, Y. Liang, H.-E. Wang, J. Li, N. Li, D. Qian, *J. Power Sources* **2021**, *501*, 230003.
[126] J. Ding, T. Xia, Q. Xia, G. Li, Y. Qu, *ACS Appl. Nano Mater.* **2022**, *5*, 654–661.
[127] R. Stephanie, S. J. Patil, N. R. Chodankar, Y. S. Huh, Y. Han, T. J. Park, *Batteries & Supercaps* **2022**, DOI 10.1002/batt.202200108.
[128] Q. Wang, H. Song, W. Li, S. Wang, L. Liu, T. Li, Y. Han, *J. Power Sources* **2022**, *517*, 230737.
[129] J. Lv, Z. Liu, L. Zhang, K. Li, S. Zhang, H. Xu, Z. Mao, H. Zhang, J. Chen, G. Pan, *Chem. Eng. J.* **2022**, *427*, 130823.
[130] J. Bonastre, J. Molina, F. Cases, *J. Energy Storage* **2023**, *69*, 107936.
[131] K. Zhou, H. Wang, J. Jiu, J. Liu, H. Yan, K. Suganuma, *Chem. Eng. J.* **2018**, *345*, 290–299.
[132] N. P. S. Chauhan, S. Jadoun, B. S. Rathore, M. Barani, P. Zarrintaj, *J. Energy Storage* **2021**, *43*, 103218.
[133] H. Li, J. Wang, Q. Chu, Z. Wang, F. Zhang, S. Wang, *J. Power Sources* **2009**, *190*, 578–586.
[134] F. Fusalba, P. Gouérec, D. Villers, D. Bélanger, *J. Electrochem. Soc.* **2001**, *148*, A1.
[135] Y.-T. Tan, F. Ran, L.-R. Wang, L.-B. Kong, L. Kang, *J. Appl. Polym. Sci.* **2013**, *127*, 1544–1549.
[136] D. S. Dhawale, A. Vinu, C. D. Lokhande, *Electrochim. Acta* **2011**, *56*, 9482–9487.
[137] K. Wang, J. Huang, Z. Wei, *J. Phys. Chem. C* **2010**, *114*, 8062–8067.

[138] K. S. Ryu, K. M. Kim, N.-G. Park, Y. J. Park, S. H. Chang, *J. Power Sources* **2002**, *103*, 305–309.
[139] W. Wu, D. Pan, Y. Li, G. Zhao, L. Jing, S. Chen, *Electrochim. Acta* **2015**, *152*, 126–134.
[140] B. Ma, X. Zhou, H. Bao, X. Li, G. Wang, *J. Power Sources* **2012**, *215*, 36–42.
[141] J. Zhang, X. S. Zhao, *J. Phys. Chem. C* **2012**, *116*, 5420–5426.
[142] P. Liao, Y. Zeng, Z. Qiu, S. Hao, J. He, H. Xu, S. Chen, *J. Alloys Compd.* **2023**, *948*, 169593.
[143] J. Fu, J. Yun, S. Wu, L. Li, L. Yu, K. H. Kim, *ACS Appl. Mater. Interfaces* **2018**, *10*, 34212–34221.
[144] J. Han, Q. Ding, C. Mei, Q. Wu, Y. Yue, X. Xu, *Electrochim. Acta* **2019**, *318*, 660–672.
[145] J. Zhou, Q. Kang, S. Xu, X. Li, C. Liu, L. Ni, N. Chen, C. Lu, X. Wang, L. Peng, X. Guo, W. Ding, W. Hou, *Nano Res.* **2022**, *15*, 285–295.
[146] C.-Y. Kung, T.-L. Wang, H.-Y. Lin, C.-H. Yang, *J. Power Sources* **2021**, *490*, 229538.
[147] J. Li, S. Qiu, B. Liu, H. Chen, D. Xiao, H. Li, *J. Power Sources* **2021**, *483*, 229219.
[148] X. Liang, L. Zhao, Q. Wang, Y. Ma, D. Zhang, *Nanoscale* **2018**, *10*, 22329–22334.
[149] J. Zhao, Y. Li, X. Chen, H. Zhang, C. Song, Z. Liu, K. Zhu, K. Cheng, K. Ye, J. Yan, D. Cao, G. Wang, X. Zhang, *Electrochim. Acta* **2018**, *292*, 458–467.
[150] P. Li, Z. Jin, L. Peng, F. Zhao, D. Xiao, Y. Jin, G. Yu, *Adv. Mater.* **2018**, *30*, 1800124.
[151] F. Lai, Z. Fang, L. Cao, W. Li, Z. Lin, P. Zhang, *Ionics* **2020**, *26*, 3015–3025.
[152] W. Li, X. Li, X. Zhang, J. Wu, X. Tian, M.-J. Zeng, J. Qu, Z.-Z. Yu, *ACS Appl. Energ. Mater.* **2020**, *3*, 9408–9416.
[153] H. Huang, S. C. Abbas, Q. Deng, Y. Ni, S. Cao, X. Ma, *J. Power Sources* **2021**, *498*, 229886.
[154] F. Niu, X. Han, H. Sun, Q. Li, X. He, Z. Liu, J. Sun, Z. Lei, *ACS Sustainable Chem. Eng.* **2021**, *9*, 4146–4156.
[155] F. Fu, H. Wang, D. Yang, X. Qiu, Z. Li, Y. Qin, *J. Colloid Interface Sci.* **2022**, *617*, 694–703.
[156] H. Xu, Z. Lei, M. Xu, J. Zhu, X. Song, X. Jin, *Int. J. Biol. Macromol.* **2023**, *236*, 123934.
[157] Y. Shen, N. Liu, J. Liu, J. Dong, S. Hu, Z. Qin, *J Energy Storage* **2023**, *63*, 106976.
[158] J. Xu, J. Ding, X. Zhou, Y. Zhang, W. Zhu, Z. Liu, S. Ge, N. Yuan, S. Fang, R. H. Baughman, *J. Power Sources* **2017**, *340*, 302–308.
[159] D. Salinas-Torres, J. M. Sieben, D. Lozano-Castelló, D. Cazorla-Amorós, E. Morallón, *Electrochim. Acta* **2013**, *89*, 326–333.
[160] Sutarsis, J. Patra, C.-Y. Su, J. Li, D. Bresser, S. Passerini, J.-K. Chang, *ACS Appl. Mater. Interfaces* **2020**, *12*, 32797–32805.
[161] M. G. Mohamed, S. V. Chaganti, M.-S. Li, M. M. Samy, S. U. Sharma, J.-T. Lee, M. H. Elsayed, H.-H. Chou, S.-W. Kuo, *ACS Appl. Energ. Mater.* **2022**, *5*, 6442–6452.
[162] L. Li, F. Lu, R. Xue, B. Ma, Q. Li, N. Wu, H. Liu, W. Yao, H. Guo, W. Yang, *ACS Appl. Mater. Interfaces* **2019**, *11*, 26355–26363.
[163] R. Xue, Y.-P. Zheng, D.-Q. Qian, D.-Y. Xu, Y.-S. Liu, S.-L. Huang, G.-Y. Yang, *Mater. Lett.* **2022**, *308*, 131229.
[164] A. F. M. EL-Mahdy, Y.-H. Hung, T. H. Mansoure, H.-H. Yu, Y.-S. Hsu, K. C. W. Wu, S.-W. Kuo, J. Taiwan Inst, *Chem. Eng.* **2019**, *103*, 199–208.
[165] S. Bandyopadhyay, C. Singh, P. Jash, W. Hussain, A. Paul, A. Patra, *Chem. Commun.* **2018**, *54*, 6796–6799.
[166] Y. Zhang, L. Cheng, L. Zhang, D. Yang, C. Du, L. Wan, J. Chen, M. Xie, *J. Energy Storage* **2021**, *34*, 102018.
[167] H. Zhang, X. Tang, C. Gu, *J. Mater. Chem. A* **2021**, *9*, 4984–4989.
[168] L. Liu, D. Cui, S. Zhang, W. Xie, C. Yao, Y. Xu, *Dalton Trans.* **2023**, *52*, 2762–2769.
[169] B. Ambrose, K. Nasrin, M. Arunkumar, A. Kannan, M. Sathish, M. Kathiresan, *J. Energy Storage* **2023**, *61*, 106714.
[170] D. Hu, Y. Jia, S. Yang, F. Huang, Y. Dong, P. Du, *J. Ind. Eng. Chem.* **2023**, *123*, 320–329.
[171] F. Xie, W. Hu, L. Ding, K. Tian, Z. Wu, L. Li, *Polym. Chem.* **2017**, *8*, 6106–6111.
[172] R. Vinodh, R. S. Babu, C. V. V. M. Gopi, C. Deviprasath, R. Atchudan, L. M. Samyn, A. L. F. de Barros, H.-J. Kim, M. Yi, *J. Energy Storage* **2020**, *28*, 101196.
[173] B. C. Patra, S. Khilari, L. Satyanarayana, D. Pradhan, A. Bhaumik, *Chem. Commun.* **2016**, *52*, 7592–7595.
[174] Y. Dong, Y. Wang, X. Zhang, Q. Lai, Y. Yang, *Chem. Eng. J.* **2022**, *449*, 137858.
[175] R. Iqbal, M. K. Majeed, A. Hussain, A. Ahmad, M. Ahmad, B. Jabar, A. R. Akbar, S. Ali, S. Rauf, A. Saleem, *Mater. Chem. Front.* **2023**, *7*, 2464–2474.
[176] X. Xu, Z. Zhang, R. Xiong, G. Lu, J. Zhang, W. Ning, S. Hu, Q. Feng, S. Qiao, *Nano-Micro Lett.* **2023**, *15*, 25.
[177] H.-C. Yang, Y.-Y. Chen, S.-Y. Suen, R.-H. Lee, *Polymer* **2023**, *273*, 125853.
[178] W.-J. Li, M. Tu, R. Cao, R. A. Fischer, *J. Mater. Chem. A* **2016**, *4*, 12356–12369.
[179] C. Lu, T. Ben, S. Xu, S. Qiu, *Angew. Chem. Int. Ed.* **2014**, *53*, 6454–6458.
[180] P. Pachfule, D. Shinde, M. Majumder, Q. Xu, *Nat. Chem.* **2016**, *8*, 718–724.
[181] D. Feng, T. Lei, M. R. Lukatskaya, J. Park, Z. Huang, M. Lee, L. Shaw, S. Chen, A. A. Yakovenko, A. Kulkarni, J. Xiao, K. Fredrickson, J. B. Tok, X. Zou, Y. Cui, Z. Bao, *Nat. Energy* **2018**, *3*, 30–36.
[182] M. Shi, R. Wang, L. Li, N. Chen, P. Xiao, C. Yan, X. Yan, *Adv. Funct. Mater.* **2023**, *33*, 2209777.
[183] J. Huang, R. B. Kaner, *Angew. Chem. Int. Ed.* **2004**, *43*, 5817–5821.
[184] A. Rudge, I. Raistrick, S. Gottesfeld, J. P. Ferraris, *Electrochim. Acta* **1994**, *39*, 273–287.
[185] A. Laforgue, P. Simon, J. F. Fauvarque, J. F. Sarrau, P. Lailler, *J. Electrochem. Soc.* **2001**, *148*, A1130.
[186] Y. Li, B. Wang, H. Chen, W. Feng, *J. Power Sources* **2010**, *195*, 3025–3030.
[187] F. Niu, R. Guo, L. Dang, J. Sun, Q. Li, X. He, Z. Liu, Z. Lei, *ACS Appl. Energ. Mater.* **2020**, *3*, 7794–7803.
[188] X. Chen, C. Zhu, F. Jiang, G. Liu, C. Liu, Q. Jiang, J. Xu, J. An, P. Liu, *J. Colloid Interface Sci.* **2021**, *601*, 265–271.
[189] S. R. P. Gnanakan, N. Murugananthem, A. Subramania, *Polym. Adv. Technol.* **2011**, *22*, 788–793.
[190] K. Wu, J. Zhao, R. Wu, B. Ruan, H. Liu, M. Wu, *J. Electroanal. Chem.* **2018**, *823*, 527–530.
[191] A. A. Advincula, A. L. Jones, K. J. Thorley, A. M. Österholm, J. F. Ponder, J. R. Reynolds, *Chem. Mater.* **2022**, *34*, 4633–4645.
[192] M. Leng, N. Koripally, J. Huang, A. Vriza, K. Y. Lee, X. Ji, C. Li, M. Hays, Q. Tu, K. Dunbar, J. Xu, T. N. Ng, L. Fang, *Mater. Horiz.* **2023**, 10.1039.D3MH00883E.
[193] Y.-J. Shao, T.-C. Yen, C.-C. Hu, G.-S. Liou, *J. Mater. Chem. A* **2023**, *11*, 1877–1885.
[194] S. Halder, S. Garg, C. Chakraborty, *Chem. Eng. J.* **2023**, *470*, 144361.
[195] R. Pal, S. L. Goyal, I. Rawal, A. K. Gupta, J. Ruchi, *Phys. Chem. Solids* **2021**, *154*, 110057.
[196] C. Fu, H. Zhou, R. Liu, Z. Huang, J. Chen, Y. Kuang, *Mater. Chem. Phys.* **2012**, *132*, 596–600.
[197] R. B. Ambade, S. B. Ambade, N. K. Shrestha, Y.-C. Nah, S.-H. Han, W. Lee, S.-H. Lee, *Chem. Commun.* **2013**, *49*, 2308.
[198] S. K. Yadav, R. Kumar, A. K. Sundramoorthy, R. K. Singh, C. M. Koo, *RSC Adv.* **2016**, *6*, 52945–52949.
[199] A. ur Rahman, H. Noreen, Z. Nawaz, J. Iqbal, G. Rahman, M. Yaseen, *New J. Chem.* **2021**, *45*, 16187–16195.
[200] R. Ravit, J. Abdullah, I. Ahmad, Y. Sulaiman, *Carbohydr. Polym.* **2019**, *203*, 128–138.
[201] I. S. Vasil'eva, G. P. Shumakovich, M. E. Khlupova, R. B. Vasiliev, V. V. Emets, V. A. Bogdanovskaya, O. V. Morozova, A. I. Yaropolov, *RSC Adv.* **2020**, *10*, 33010–33017.
[202] P. Zhang, Y. Li, M. Gao, S. Yang, M. Wang, Z. Liu, K. Guo, F. Wang, X. Lu, *Chem. Eng. J.* **2023**, *454*, 140357.
[203] K. Balakrishnan, M. Kumar, S. Angaiah, *Adv. Mater. Res.* **2014**, *938*, 151–157.
[204] L. Manjakkal, A. Pullanchiyodan, N. Yogeswaran, E. S. Hosseini, R. Dahiya, *Adv. Mater.* **2020**, *32*, 1907254.
[205] H. Mu, W. Wang, L. Yang, J. Chen, X. Li, Y. Yuan, X. Tian, G. Wang, *Energy Storage Mater.* **2021**, *39*, 130–138.
[206] R. B. Ambade, S. B. Ambade, R. R. Salunkhe, V. Malgras, S.-H. Jin, Y. Yamauchi, S.-H. Lee, *J. Mater. Chem. A* **2016**, *4*, 7406–7415.
[207] J. H. Won, M. Latifatu, M. Jang, H. S. Lee, B.-C. Kim, L. Hamenu, J. H. Park, K. M. Kim, J. M. Ko, *Synth. Met.* **2015**, *203*, 31–36.
[208] M. Sun, G. Wang, C. Yang, H. Jiang, C. Li, *J. Mater. Chem. A* **2015**, *3*, 3880–3890.
[209] X.-G. Li, H. Li, M.-R. Huang, *Chem. Eur. J.* **2007**, *13*, 8884–8896.
[210] C. Yang, M. Sun, X. Wang, G. Wang, *ACS Sustainable Chem. Eng.* **2015**, *3*, 2067–2076.
[211] Z. Yang, J. Liu, Y. Li, G. Zhang, G. Xing, L. Chen, *Angew. Chem. Int. Ed.* **2021**, *60*, 20754–20759.
[212] A. F. M. El-Mahdy, Y. Hung, T. H. Mansoure, H. Yu, T. Chen, S. Kuo, *Chem. Asian J.* **2019**, *14*, 1429–1435.

[213] C. Weng, X. Li, Z. Yang, H. Long, C. Lu, L. Dong, S. Zhao, L. Tan, *Chem. Commun.* **2022**, *58*, 6809–6812.
[214] J. C. Bachman, R. Kavian, D. J. Graham, D. Y. Kim, S. Noda, D. G. Nocera, Y. Shao-Horn, S. W. Lee, *Nat. Commun.* **2015**, *6*, 7040.
[215] E. Grodzka, K. Winkler, B. M. Esteban, C. Kvarnstrom, *Electrochim. Acta* **2010**.
[216] J. Huang, K. Jiang, D. Tranca, C. Ke, L. Zhang, J. Li, J. Li, G. Tong, E. Kymakis, X. Zhuang, *J. Appl. Polym. Sci.* **2021**, *138*, 51198.
[217] Z. Gan, J. Yin, X. Xu, Y. Cheng, T. Yu, *ACS Nano* **2022**, *16*, 5131–5152.
[218] H. Lindström, S. Södergren, A. Solbrand, H. Rensmo, J. Hjelm, A. Hagfeldt, S.-E. Lindquist, *J. Phys. Chem. B* **1997**, *101*, 7717–7722.
[219] J. E. B. Randles, *Trans. Faraday Soc.* **1948**, *44*, 327.

Manuscript received: July 1, 2023
Revised manuscript received: August 30, 2023
Accepted manuscript online: August 31, 2023
Version of record online: September 15, 2023